Transportation Research Part B 113 (2018) 143–163

Contents lists available at ScienceDirect

Transportation Research Part B

journal homepage: www.elsevier.com/locate/trb

Effects of maximum relaxation in viscoelastic traffic flow modeling

Jian Ma[a,c], C.K. Chan[b], Zhongbao Ye[a], Zuojin Zhu[a,b,*]

[a] Faculty of Engineering Science, University of Science and Technology of China, Hefei 230026, China
[b] Department of Applied Mathematics, The Hong Kong Polytechnic University, Hung Hom, Kowloon, Hong Kong
[c] Naval Architecture and Civil Engineering, Jiangsu University of Science and Technology, Jiangsu Province 215600, China

ARTICLE INFO

Article history:
Received 30 March 2017
Revised 25 March 2018
Accepted 21 May 2018

Keywords:
Viscoelastic modeling
Ring road traffic flow
Spatial-temporal patterns
Shock and rarefaction waves

ABSTRACT

Viscoelastic modeling is used to describe traffic flows in analogous to non-Newtonian fluid flows, where first and second order linear viscoelastic approximations are employed. This paper presents the effects of maximum relaxation in traffic flow modeling by demonstrating numerical results of single lane ring road traffic flows. Numerical results show that there is a wide spectrum of spatial-temporal pattern formation phenomena in traffic system. Self-organization plays a crucial role in the determination of traffic flow patterns and a different initial density causes a completely distinct traffic flow pattern. Predicting traffic flow acceleration is useful for checking reliability of the simulation and maximum relaxation brings about some observable but non-significant effects on traffic flow patterns.

1. Introduction

In a modern world, the growth of highway networks between cities and widening of road traffic have become channels of transport logistics between cities, and urban/rural areas. It has great impact on development of urban and rural economies. Therefore, traffic flows have been extensively studied, resulting in the occurrence of many traffic flow models, among which the Lighthill–Whitham–Richards (LWR) model (Lighthill and Whitham, 1955; Richards, 1956) is the simplest and is capable of capturing crucial flow features of highways and predicting traffic shock waves with relatively steep wave fronts as reported by Kühne and Michalopoulos (2001). It has been extended to describe a behavioral theory of multi-lane traffic flow (Daganzo, 2002a; 2002b), to predict traffic hysteresis (Wong and Wong, 2002), evolution of traffic waves (Zhu and Wu, 2003) and critical transition of traffic flow bottlenecks (Chang and Zhu, 2006).

Furthermore, Euler model (Payne, 1971), gas-kinetic-based model (Helbing and Treiber, 1998; Hoogendoorn and Bovy, 2000), cluster effect model (Kerner and Konhäuser, 1993), and generic model (Lebacque, et al., 2007; Zhang, et al., 2009; Lebacque and Khoshyaran, 2013) have been proposed. High-order models have also been used to explain the vehicular flow phenomena and traffic wave spreadings successfully.

Despite some critical comments (Daganzo, 1995), there were many remarkable applications (Jin and Zhang, 2003; Greenberg, 2004; Zhang and Wong, 2006; Xu, et al., 2007; Ou, et al., 2007; Qiao, et al., 2014) and developments (Klar and Wegener, 2000; Aw and Rascle, 2000; Kiselev, et al., 2000a; Zhang, 2003; Lebacque, et al., 2007; Zhang, et al., 2009; Mammar, et al., 2009; Ngoduy, 2012, 2013; Zhu and Yang, 2013; Spiliopoulou, et al., 2014, 2015; Bogdanova, et al., 2015; Hoogendoorn, et al., 2015; Smirnova, et al., 2016, 2017). Patterns of traffic flows have been mathematically described by car-following mod-

* Corresponding author at: Faculty of Engineering Science, University of Science and Technology of China, Hefei 230026, China.
E-mail address: zuojin@ustc.edu.cn (Z. Zhu).

https://doi.org/10.1016/j.trb.2018.05.013
0191-2615/

els, cellular automaton models (Nagel and Schreckenberg, 1992; Helbing and Huberman, 1998; Chowdhury, et al., 2000), gas-kinetic models and fluid-dynamical models (Nagatani, 2002).

By using the concepts of Lagrangian mass coordinate and anticipatory acceleration, Greenberg (2004) has analyzed a class of second-order traffic models, and found that these models support stable oscillatory traveling waves typically observed on a congested roadway. With the gas-kinetic based approach (Helbing and Treiber, 1998; Hoogendoorn and Bovy, 2000; Ngoduy, 2012), a macroscopic model has been developed (Ngoduy, 2013) to describe the traffic flow where intelligent vehicles move close to each other as compared with manual vehicles and operate in a form of many platoons each of which contains several vehicles. A stochastic conservative model in continuous time over discrete space, following a misanthrope Markovian process has been studied by Tordeux et al. (2014). It was reported (Lebacque and Khoshyaran, 2013) that with the generic second order model (GSOM), the family of traffic models can be expressed as a system of conservation laws; a proper Lagrangian formulation of the GSOM model can then be reformulated as a Hamilton–Jacobi equation, the solution of which can be expressed as the value function of an optimal control problem. For models of the GSOM family, an adequate framework for effective numerical methods has been obtained (Costeseque and Lebacque, 2014).

Xu, et al. (2007) have analytically investigated a wide cluster solution of Euler type traffic flow models and found that it is not admitted in some traffic flow models in literatures. For those models which admit the wide cluster solution, they thoroughly discussed the relationship between two important control parameters and the critical densities which divide an equilibrium solution into stable and unstable regions.

A novel formulation of non-equilibrium traffic flow models based on their isomorphic relation with optimal control problems was given by Li and Zhang (2013). It demonstrated that with the new formulation, generic initial-boundary conditions can be conveniently handled so that a simplified numerical scheme for non-equilibrium models can be devised.

In this paper, first order viscoelastic traffic flow models (Smirnova, et al., 2014a; Bogdanova, et al., 2015) and second order linear viscoelastic approximation (Zhu and Yang, 2013) are described. Both models are validated by the model derived from the car-following rule (Zhang, 2003), and numerical results are obtained with the same road operational conditions. With viscoelastic models, the effects of maximum relaxation in traffic flow modeling with numerical tests for ring road traffic flows are investigated. For cases of fixed vehicle length l , braking distance X_{br}, and characteristic length of flows l_0, with different viscoelasticity γ, and initial density distribution characterized by ρ_0/ρ_m, the effects on density, speed and their fluctuations on the ring road are compared with available measured data.

2. Viscoelastic models

In viscoelastic traffic flow modeling, an analogy to linear viscoelastic fluid flow is used, in which shear stress is given by

$$\mathbf{T}_s = \int_0^\infty f(s)\mathbf{H}(s)ds, \tag{1}$$

where $f(s)$ is a memory function. With experimental observation of the relaxation of shear stress of macromolecular polymer and theory of micro-rheology (Wagner, 1978), the memory function $f(s)$ may be written in the form of

$$f(s) = G\sum_1^N \frac{1}{\tau_j}\exp\left(-s/\tau_j\right), \tag{2}$$

where G denotes the modulus of fluid elasticity, τ_j represents the jth order relaxation time.

As reported by Daganzo (1995), vehicles mainly react to downstream traffic conditions instead of prevailing traffic conditions and slow vehicles virtually remain unaffected by fast vehicles. These properties led to the derivation of a third dynamic equation for velocity variance (Helbing, 1996), as reported in the continuum modeling of multi-class traffic flow (Hoogendoorn and Bovy, 2000). In the present viscoelastic traffic flow model, driver behavior has not been considered in detail as in the multiclass generalization of the single-class gas-kinetic equation (Paveri-Fontana, 1975) by Hoogendoorn and Bovy (2000). Vehicles are only taken as linear viscoelastic fluid particles, with the complicated vehicular movement described by pressure and viscoelasticity used in fluid mechanics.

In this paper, several assumptions are made in discussing the effects of maximum relaxation; namely (i) ramp flow effect is neglected; (ii) road capacity is insensitive to the drivers; (iii) vehicles are treated as linear viscoelastic fluid particles (Zhu and Yang, 2013; Smirnova, et al., 2014a; Bogdanova, et al., 2015).

The constitutive equation of a general linear viscoelastic fluid flow is given by

$$\mathbf{T} = -p\mathbf{I} + G\sum_{j=1}^N \int_0^\infty \frac{1}{\tau_j}\exp(-s/\tau_j)\mathbf{H}(s)ds, \tag{3}$$

where $\mathbf{T}(= -p\mathbf{I} + \mathbf{T}_s)$ and p are stress tensor and traffic pressure respectively and $\mathbf{H}(s)$ is the Finger deformation tensor. For the maximum relaxation order denoted by N, the Finger deformation tensor is given by $\mathbf{H}(s) = \sum_{k=1}^N (-1)^{k+1}\frac{s^k}{k!}\mathbf{B}_k$, where $\mathbf{B}_k$ is the White-Metzner tensor, and s is the elapsed time period as given by Han (2000).

Traffic pressure p has been employed in Payne-type models (Payne, 1971, 1979) to remedy the LWR model (Lighthill and Whitham, 1955; Richards, 1956). Drawback of the LWR model includes complete admission of the traffic fundamental diagram, inability to capture the formation of local structures, phantom-jams, hysteresis, and stop-start waves under specific traffic conditions. In addition, discontinuous solutions result irrespective of smoothness of the initial solutions (Lyrintzis, et al., 1994; Kerner, et al., 1996; Hoogendoorn and Bovy, 2000). The traffic pressure was treated as a linear function of traffic density in the work of Liu, Lyrintzis and Michalopoulos (1996), which was assumed to have a general function of traffic density in the nonequilibrium traffic flow model (Zhang, 1998).

In the macroscopic gas-kinetic-based tr affic flow model (GKT model) (Helbing and Treiber, 1998; Treiber, Hennecke and Helbing, 1999), traffic pressure was considered as a product of traffic density and velocity variance θ, i.e., $p = \rho\theta$, where $\theta = A(\rho)u_e^2$, with $A(\rho)$ being an empirical function of traffic density ρ, as also seen in Delis, et al. (2014). In the traffic flow model of Aw and Rascle (2000), similar to an expression used in gas dynamics, $p \propto \rho^{\kappa}$ was suggested, where κ is a positive constant to be determined be means of nonlinear analysis (Ou, et al. 2007). In particular, in the class of second-order traffic models analyzed by Greenberg (2004), the traffic pressure-gradient term is alternated by the anticipatory acceleration.

By further studying the relationship between microscopic car-following and macroscopic fluid-like behavior of traffic flow, a second-order continuum model with viscosity was developed (Zhang, 2003). In the conserved higher-order anisotropic traffic flow model (Zhang, Wong and Dai, 2009), a pseudo-density transformed from velocity is introduced. In particular, traffic viscosity effect is completely ignored, and pressure is taken as a function of the pseudo-density and the relaxation of velocity to equilibrium. It was mentioned that in traffic flow modeling, different choices for the pressure and fundamental diagram are possible, as traffic flow is a very complicated system of self-driven particles (Helbing, 2001), implying that a given choice for the pressure and fundamental diagram is suitable to a certain scenario only. In generic second order modeling (Lebacque and Khoshyaran, 2013), the velocity equation is replaced by a governing equation of driver attribute I, with the driver dependent fundamental diagram given by $\Re(\rho, I) = \rho\Im(\rho, I)$, without adopting the concept of traffic pressure which is just a notation, but does not exist physically (Smirnov, et al., 2014; Smirnova, et al., 2017).

As suggested by Zhu and Yang (2013), using second-order approximation (N=2) , and the expression $\int_0^\infty s^k \exp(-as)ds = \frac{k!}{a^{k+1}}$, the traffic flow stress can be expressed as:

$$T = -p + G(\tau_1 + \tau_2)B_1 - G(\tau_1^2 + \tau_2^2)B_2, \tag{4}$$

As described by Han (2000), $B_1 = 2u_x$ and

$$B_2 = B_{1t} + uB_{1x} - 2B_1^2. \tag{5}$$

Since τ_j can be approximated by τ_1/j^2, the total relaxation time can be approximated as $\tau \approx \tau_1 + \tau_2 = 1.25\tau_1$, such that $\tau_1 = 0.8\tau$, and $\tau_2 = 0.2\tau$. Noting that fluid elasticity is given by $\sigma = 2G(\tau_1^2 + \tau_2^2)/\rho$, dynamic viscosity is given by $\mu = \rho\nu = 2G\tau$, we can express elasticity as $\sigma = \nu(\tau_1^2 + \tau_2^2)/\tau$, or

$$\sigma = \nu(\tau - 2\tau_1\tau_2/\tau) = 0.68\nu\tau. \tag{6}$$

According to traditional traffic flow modeling, the general form of the force acting on vehicular clusters can be formulated as

$$F = (q_e - q)/\tau + T_x, \tag{7}$$

where q_e is the flow rate under the equilibrium traffic state, and T_x is the relevant surface force related to the traffic flow stress.

Based on the traffic fundamental diagram used by Kiselev et al. (2000b), for further modifying the traffic flow rate q_e at density beyond second critical value ρ_{c2}, denoting the second critical speed of traffic flow by $u_{c2}(\rho_{c2}) = c_\tau/\Lambda$, then q_e can be written as

$$q_e = \begin{cases} v_f\rho, & \text{for } \rho \le \rho_*, \\ -c_\tau\rho\ln(\rho/\rho_m), & \text{for } \rho_* < \rho \le \rho_{c2}, \\ B\rho\{1 - \operatorname{sech}[\Lambda\ln(\rho/\rho_m)]\}, & \text{for } \rho_{c2} < \rho \le \rho_m, \end{cases} \tag{8}$$

where $\rho_{c2}/\rho_m = \exp(-1/\Lambda)$, and $B = u_{c2}/\{1 - \operatorname{sech}[\Lambda\ln(\rho_{c2}/\rho_m)]\}$, depends not only on the second critical density and speed but also on the speed ratio Λ and jam density ρ_m. The density dependance of equilibrium flow q_e is postulated according to the flow peculiarity that any flow state in over the 2nd critical traffic is dominated by jams propagation and interactions with spontaneously generated jam and rarefaction waves. The maximum permissible density ρ_* at free flow speed v_f is

$$\rho_* = \rho_m\exp(-v_f/c_\tau). \tag{9}$$

As safe traffic density itself implies that the distance between vehicles are not shorter than the braking distance $X_{\rm br}$, the density ρ_* is then defined by the equality

$$\rho_* = \rho_m[1 + X_{\rm br}/l]^{-1}, \tag{10}$$

which is generally referred to as 1st critical density or 1st transitional density. Combining Eqs. (9) and (10), we obtain

$$c_\tau = v_f/\ln[1 + X_{\rm br}/l]. \tag{11}$$

The traffic state Eq. (8) is shown in Fig. 1, where ρ_{c2} is the 2nd critical traffic density, above which traffic flow becomes stable again.

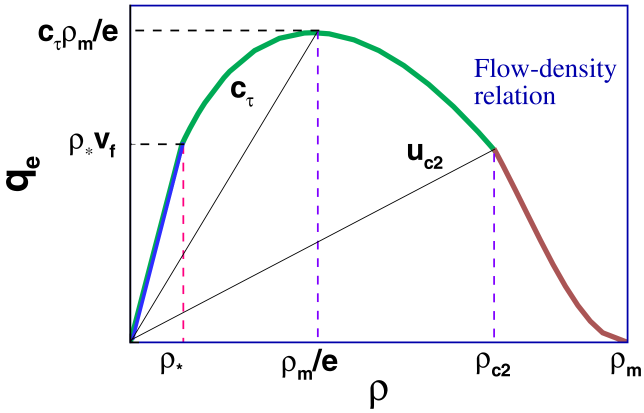

Fig. 1. Fundamental diagram given by Eq. (8).

It is noted that at ρ_* and ρ_{c2}, the function or the kinetic speed $q_e'(\rho)$ is discontinuous, which might not bother numerical simulations but might give troublesome in the mathematics for discussion.

Traffic pressure is defined by

$$p = p_m(1-\alpha)(\rho/\rho_m)/[1-\alpha(\rho/\rho_m)], \tag{12}$$

where $\alpha = l\rho_m$, is the product of average vehicle length l and ρ_m, p_m are jam density and jam pressure respectively. It is noted that the flow-density relation used for illustrating traffic fundamental diagram, usually called traffic state equation, has a crucial impact on the traffic road operation (Haight, 1963). In addition, weather conditions, running performances of vehicles have influences on drivers' psychology and driving behaviors.

Eq. (12) is derived with the assumption that traffic pressure is proportional to the reciprocal of spatial headway of vehicles rather than traffic density directly, and sound speed of traffic flow can be derived as $c^2 = (\partial p/\partial \rho)$. Thus, denoting the proportional coefficient by K, we have

$$p = K \cdot \frac{1}{s-l}, \tag{13}$$

where $s = 1/\rho$. Using $\alpha = l\rho_m$, its equivalent form can be expressed as

$$p = \frac{K\rho}{1-\alpha\rho/\rho_m}, \tag{14}$$

when $\rho = \rho_m$, giving

$$K = (1-\alpha)p_m/\rho_m. \tag{15}$$

It can be seen that this pressure expression allows the speed of sound to be calculated from

$$c^2 = \frac{K}{[1-\alpha\rho/\rho_m]^2}. \tag{16}$$

If the sound speed at second critical density ρ_{c2} has a value which is identical to $-\rho[u_e']\big|_{\rho_{c2}} = c_\tau$, then we have (Zhang, 2003)

$$K = \{c_\tau[1-\alpha\rho_{c2}/\rho_m]\}^2. \tag{17}$$

Putting $c_0 = c_\tau$, Eq. (16) can be rewritten as

$$\frac{c}{c_0} = \frac{1-\alpha\rho_{c2}/\rho_m}{1-\alpha\rho/\rho_m}, \tag{18}$$

implying that

$$\frac{d(c/c_0)}{d(\rho/\rho_m)} = \frac{c}{c_0} \cdot \left(\frac{\alpha}{1-\alpha\rho/\rho_m}\right), \tag{19}$$

and

$$p = c_0^2\rho \cdot \left(\frac{[1-\alpha\rho_{c2}/\rho_m]^2}{1-\alpha\rho/\rho_m}\right). \tag{20}$$

As spatial headway $(s-l)$ tends to zero, the traffic pressure $p \to \infty$, implying that local vehicle stoppages or unexpected local vehicle collisions are inevitable. In this paper, we show the traffic flow acceleration evolution at some fixed sections. It is more direct and convenient to determine whether traffic acceleration has exceeded the empirical limits $(-5\,\mathrm{m/s^2}, 1.5\,\mathrm{m/s^2})$ (Smirnova, et al., 2015), and also whether traffic flows have been simulated reliably.

With the definition $q = \rho u$, $B_1 = 2u_x$, and the expression of vehicular mass conservation $\rho_t + q_x = 0$ under the assumption (i), as described by Han (2000), ρB_2 has the form

$$\begin{aligned} \rho B_2 &= \rho B_{1t} + \rho u B_{1x} - 2\rho B_1^2, \\ &= 2\rho(u_t + uu_x)_x - 6\rho u_x^2, \end{aligned} \tag{21}$$

such that

$$T = -p + (\rho\nu + \mu_1)u_x - \rho\sigma(u_t + uu_x)_x, \tag{22}$$

where $\mu_1 = 3\rho\sigma u_x = \rho\nu_1$. Combining Eqs. (7), (12), and (22), the governing equations based on viscoelastic traffic flows modeling with maximum relaxation order $N = 2$ become

$$\begin{cases} \rho_t + q_x = 0, \\ \rho(u_t + uu_x) = R, \\ R + [\rho\sigma(R/\rho)_x]_x = \rho(u_e - u)/\tau - c^2\rho_x + [(2G\tau + \rho\nu_1)u_x]_x. \end{cases} \tag{23}$$

From Eq. (23), it is seen that the traffic acceleration R/ρ depends on pressure gradient $c^2\rho_x/\rho$, implying possible occurrences of negative speeds in the solutions, even in the cases of excluding the viscous and relaxation time related terms (Aw and Rascle, 2000). As a car is an anisotropic particle that mostly responds to frontal stimuli, not completely identical to a fluid particle, in modeling vehicular acceleration, relaxation time related term $\rho(u_e - u)/\tau$ should be included. Following the *principle* that all traffic waves connecting any state to its left must have a propagation speed (shock speed) *at most* equal to the traffic speed, anisotropic higher-order traffic flow models have been developed and studied (Rascle, 2002; Xu, et al., 2007).

In the viscoelastic traffic flow model, traffic pressure gradient results in the *principle* for shock speed mentioned above not been satisfied, as from the view of fluid mechanics it is unnecessary to limit shock speed with the speed of Brownian motion of fluid molecules. The use of relaxation term $\rho(u_e - u)/\tau$ can decrease the probability of negative speed occurrences, in particular, when geometric average of $2G\tau$ is used to set the visco-elasticity on the mesh-faces, for instance in the numerical simulation of a queue-stoppage at a traffic light with models having abandoned the *principle* for shock speed.

Similarly, in a more simple analogy to unsteady traffic flows for the case of $N = 1$ as in Smirnova, et al. (2014a) and Bogdanova, et al. (2015), the governing equations based on viscoelastic traffic flows modeling with maximum relaxation order $N = 1$ can be expressed as

$$\begin{cases} \rho_t + q_x = 0, \\ \rho(u_t + uu_x) = R, \\ R = \rho(u_e - u)/\tau - c^2\rho_x + [(2G\tau)u_x]_x. \end{cases} \tag{24}$$

Traffic flow viscosity has been employed in several well known mathematical models (Whitham, 1974; Kühne, 1987; 1989; Kerner, et al., 1996; Zhang, 2003). While Navier–Stikes equations have been used to describe all viscous flows, its use in traffic flows is not apparent. Similar to viscosity in fluid mechanics, arising from resistance to change of shear stress, it is postulated that in traffic flow it is the drivers tendency to resist sudden and sharp changes in speed that leads to viscous terms in traffic speed dynamics.

The interactions between multiple class vehicles (Hoogendoorn and Bovy, 2000) can be viewed as a primary and intrinsic reason of introducing the concept of viscoelasticity in traffic flow modeling based on the constitutive relationship of non-Newtonian fluid flow. Furthermore viscoelastic modeling of multiple class and multi-lane traffic flows is becoming common. This paper only concentrates on the effect of maximum relaxation in viscoelastic modeling of single class traffic flows, applying the models described in numerical tests for single lane ring-traffic flows.

To develop a conserved higher-order anisotropic traffic flow model, a pseudo-density is introduced (Zhang, et al., 2009), avoiding the concept of named traffic pressure and sound speed. However, ascertaining details of potential of the conserved anisotropic model needs further studies, such as the problems of initial condition of pseudo-density and the effects of pseudo-density dependent equilibrium velocity.

To represent the propagation of an infinitesimal disturbance, sound speed cannot be ignored when traffic flow is specially light (ρ=0) or completely jammed (ρ/ρ_m=1). From classical mechanics, sound speed may be defined as the isentropic derivative of pressure to density, rather than to employ the fundamental diagram of traffic flow (Payne, 1971).

To validate the reliability and applicability of viscoelastic traffic models, it is necessary to compare numerical simulations with the higher order model derived from car-following rule (Zhang, 2003) with the same initial and boundary conditions, expressions for traffic pressure and sound speed.

3. Numerical method

Taking $R_1 = R + c^2\rho_x$ instead of R, the governing Eq. (23) or (24) becomes

$$\frac{\partial \mathbf{U}}{\partial t} + \frac{\partial \mathbf{F}(\mathbf{U})}{\partial x} = \mathbf{S}, \tag{25}$$

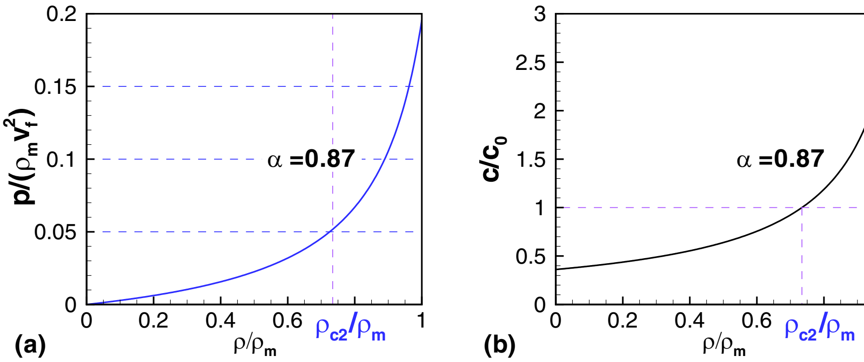

Fig. 2. Traffic pressure (a) and sound speed ratio (b) plotted as functions of density ρ. (Density and pressure are measured by ρ_m and $\rho_m v_f^2$ respectively).

Table 1
Parameters of ring road traffic operations.

v_f (km/h)	ρ_m (veh/km)	$X(v_f)$ (m)	l (m)	u_{c2}(km/h)	l_0 (m)	t_0(s)
110	150	50	5.8	15	160	50.377
τ_0(s)	c_0/v_0	ρ_*/ρ_m	Λ	x_{Imax}	x_A	x_B
11.854	4.250	0.1039	3.239	780	195	585

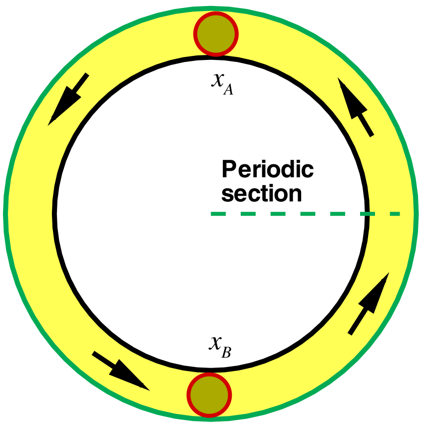

Fig. 3. Schematic diagram of ring road traffic flow without ramps.

where $\mathbf{U} = (\rho, q)^T$, $\mathbf{F}(\mathbf{U}) = (q, q^2/\rho + p)^T$, and $\mathbf{S} = (0, R_1)^T$, with superscript 'T' representing vector transpose.

The eigenvalues of Eq. (25) λ_k, $(k = 1, 2)$ may be expressed as $\lambda_1 = u - c$ and $\lambda_2 = u + c$, where the Jacobian matrix is

$$\mathbf{A} = \begin{pmatrix} \dfrac{\partial F_1}{\partial U_1} & \dfrac{\partial F_1}{\partial U_2} \\ \dfrac{\partial F_2}{\partial U_1} & \dfrac{\partial F_2}{\partial U_2} \end{pmatrix} = \begin{pmatrix} 0 & 1 \\ -u^2 + c^2 & 2u \end{pmatrix}. \tag{26}$$

While some believe that the eigenvalue should not exceed the traffic speed, the present viscoelastic model uses non-Newtonian fluid flow analogy, such that the traffic speed involves vehicular cluster rather than a single car, the eigenvalue limit is irrelevant. In fact, an eigenvalue represents the propagation speed of traffic waves (shock speed) and it is not necessary to limit the propagation speed with respect to the speed of Brownian motion of fluid molecular particles.

For numerical simulations of traffic flows, there are many methods, such as the Lax–Friedrichs scheme (Xu, et al., 2007), the weighted essentially non-oscillatory numerical scheme (WENO scheme) (Zhang, et al., 2006; Delis, etal, 2014), the discontinuous Galerkin finite element scheme (Qiao, et al., 2014), the methods used in pseudo-code design (Costeseque and Lebacque, 2014), and the total variation diminishing (TVD) scheme (Smirnova, et al., 2017), etc. To obtain numerical solutions of governing Eq. (25), the TVD scheme developed by Roe (1981) is adopted. Denoting respectively the mesh size and ratio of time step to mesh size respectively by Δx_i and $\omega = \Delta t/\Delta x$, the Courant–Friedrichs–Lewy (CFL) condition of TVD is satisfied by putting

$$\omega = C_{\mathrm{FL}}/\max|\lambda_{k,i+1/2}|, \quad k = 1, 2; \quad i = 0, 1, 2, \ldots, I_{\max} - 1, \tag{27}$$

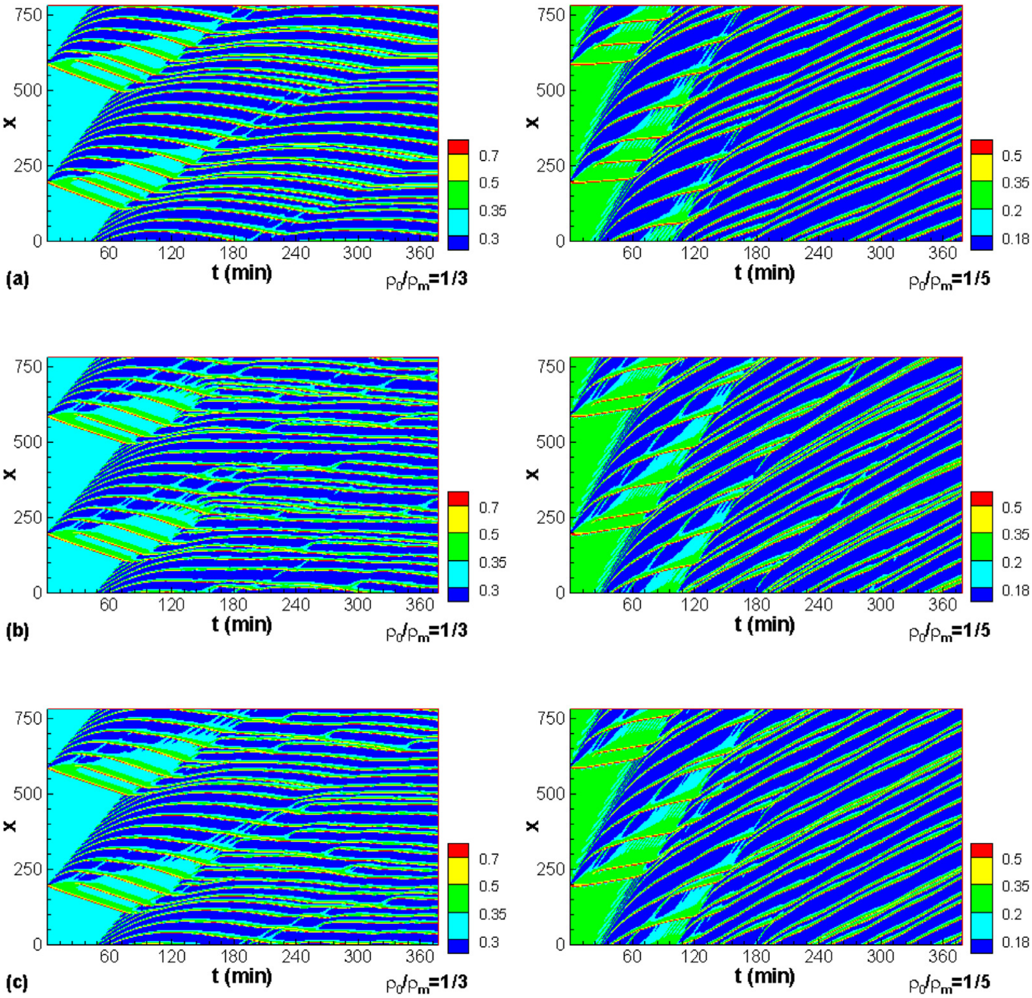

Fig. 4. Spatial-temporal evolutions of ring road traffic flow density for $\gamma = 0.125$, (a) Zhang (2003); (b) N=1; (c) N=2.

where $\lambda_{k,i+1/2}$ represents the kth eigenvalue for $\mathbf{A}$ at $x_{i+1/2}$, $I_{\max}$ is the maximum number of mesh, and the Courant number $C_{\mathrm{FL}} = 0.4$ (Shui, 1998) is fixed in the numerical tests.

Linearization of non-linear source terms is a general approach in numerical treatments (Tao, 2001). With linear expansion, the source term R_1 at the time level $t^n + 1/2$ can be calculated by

$$R_1^{n+1/2} = R_1^n + \frac{1}{2}\left(\frac{\partial R_1}{\partial \rho}\right)^n \delta\rho^n + \frac{1}{2}\left(\frac{\partial R_1}{\partial q}\right)^n \delta q^n, \tag{28}$$

where $\delta\rho^n = \rho^{n+1} - \rho^n$, $\delta q^n = q^{n+1} - q^n$. Representing the speed and length scales respectively by v_0 and $\Delta x(=l_0)$, we have time scale $t_0 = l_0/v_0$. For simplicity, using the scaled variables as the same as the unscaled, so that for $N = 1$ the form of dimensionless expression

$$\begin{aligned} R_1 &= R + c^2\rho_x \\ &= (q_e - q)/\tau + [(2G\tau)u_x]_x \end{aligned}$$

keep unchanged, by simply neglecting the roles of viscous term $[(2G\tau)u_x]_x$ in the linearization, we approximately have

$$\frac{\partial R_1}{\partial \rho} = \tau^{-1}\left(\frac{\partial q_e}{\partial \rho}\right), \quad \frac{\partial R_1}{\partial q} = -\tau^{-1}. \tag{29}$$

For $N = 2$, R_1 should satisfy the equation

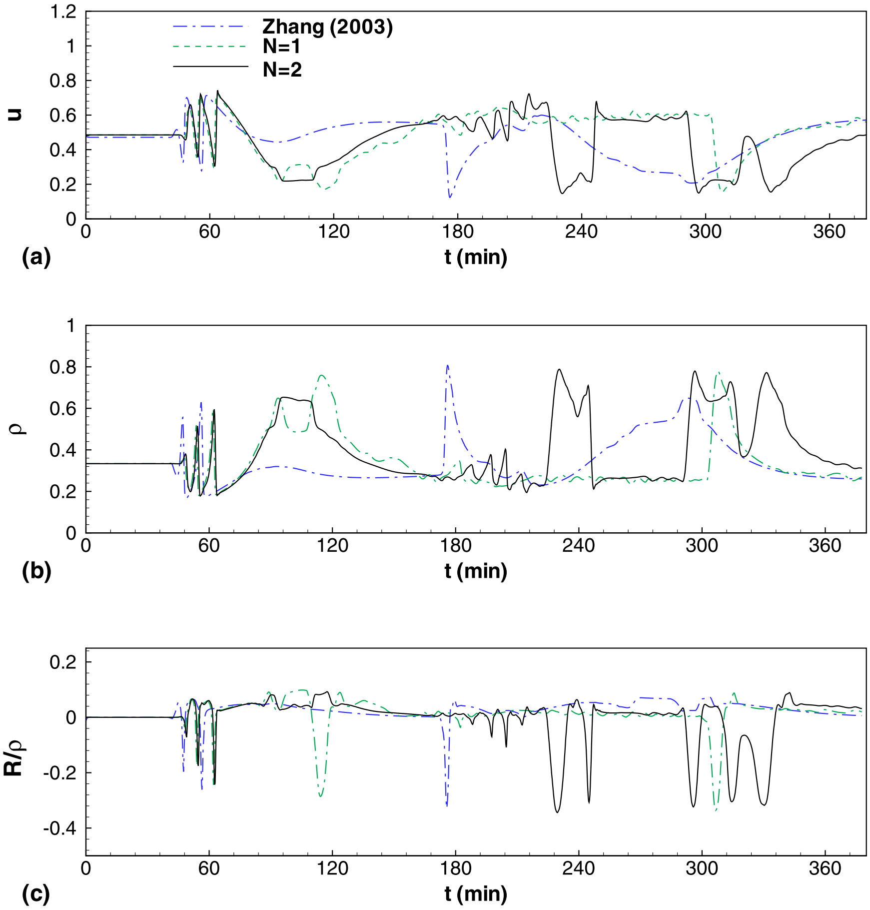

Fig. 5. Temporal evolutions of traffic flow speed (a), density (b) and acceleration (c) at x=390 for $\gamma = 0.125$, and ρ_0/ρ_m=1/3. Note that R/ρ has a unit of the permitted maximum acceleration 1.5 m/s^2 as reported by Smirnova, et al. (2015).

$$\begin{aligned} R_1 &= R + c^2\rho_x \\ &= (q_e - q)/\tau + [(2G\tau + \rho\nu_1)u_x]_x - \{\rho\sigma[(R_1 - c^2\rho_x)/\rho]_x\}_x \end{aligned} \tag{30}$$

which can be solved numerically. Similarly, by simply neglecting the roles of viscous term $[(2G\tau)u_x]_x$ and elastic terms $[\rho\nu_1 u_x]_x$ and $\{\rho\sigma[(R_1 - c^2\rho_x)/\rho]_x\}_x$, the Eq. (29) is still established approximately. The linear expansion of R_1 is just an approach to improve the temporal discretization accuracy of Eq. (25), as reported in Ref. (Sminova, et al., 2017).

The TVD scheme has the form

$$\delta\mathbf{U}_i^n = -\omega(\hat{\mathbf{F}}_{i+1/2} - \hat{\mathbf{F}}_{i+1/2}) + (\Delta t)\mathbf{S}_i^n + \frac{\Delta t}{2}\left(\frac{\partial\mathbf{S}}{\partial\mathbf{U}}\right)_i^n \delta\mathbf{U}_i^n, \tag{31}$$

where $\delta\mathbf{U}_i^n = \mathbf{U}_i^{n+1} - \mathbf{U}_i^n$, $\Delta t(= t^{n+1} - t^n)$. The numerical flux $\hat{\mathbf{F}}_{i+1/2}$ can be calculated using the eigen vectors of Jacobian matrix A. The calculation of $\hat{\mathbf{F}}_{i+1/2}$ involves evaluating the coefficients of viscous term $Q_k(z)$ with an artificial parameter ϵ_k, as outlined by Zhu and Wu (2003) and Chang and Zhu (2006).

The dependence of traffic pressure p and sound speed ratio c/c_0 on the normalized traffic density ρ/ρ_m as shown in Fig. 2 is calculated so that they can subsequently be used by linear interpolation in numerical tests. This methodology in flow simulator coding is more flexible than using explicit expressions of traffic pressure p and sound speed ratio c/c_0 directly, and thus having a wider potential in applications.

4. Model comparison

To validate the reliability and applicability of viscoelastic traffic flow models described above, the traffic flow model derived on the basis of car-following rule (Zhang, 2003) is used. By assuming $\tau_0/\tau = c/c_0$, and $l_0 = c_0\tau_0$ similar to the

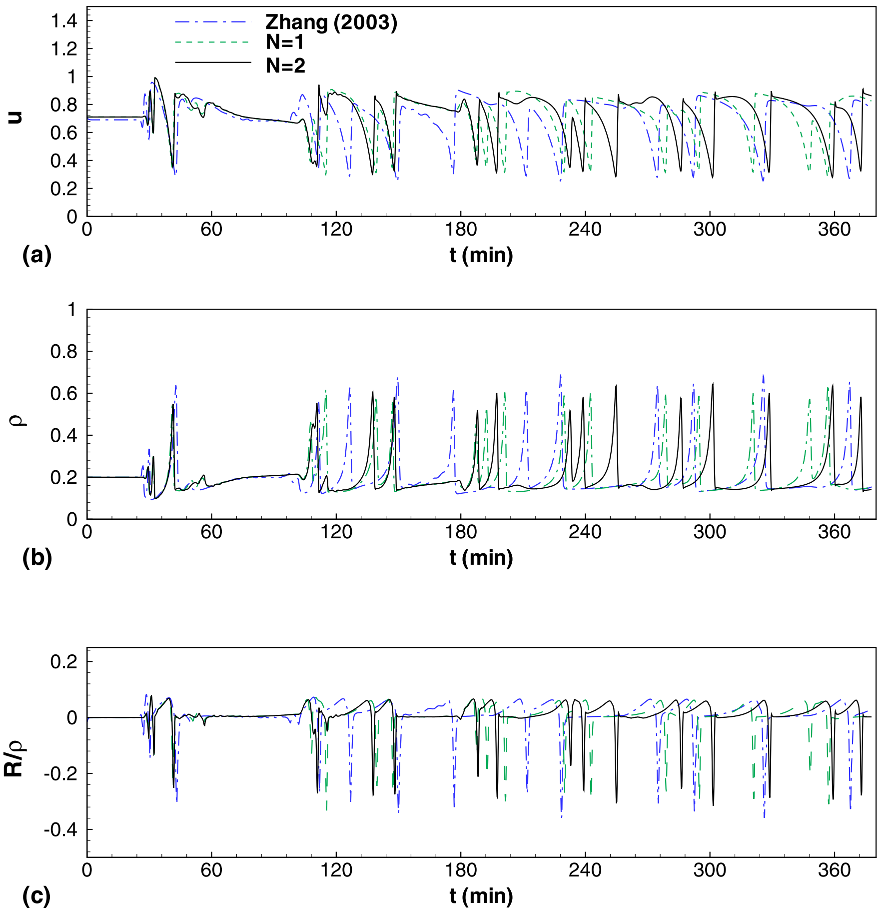

Fig. 6. Temporal evolutions of traffic flow speed (a), density (b) and acceleration (c) at x=390 for $\gamma = 0.125$, and ρ_0/ρ_m=1/3. Note that R/ρ has a unit of the permitted maximum acceleration 1.5 m/s^2 as reported by Smirnova, et al. (2015).

Table 2
Parameters adopted in numerical tests.

Case	N	ρ_0/ρ_m	$\gamma = \left[\frac{2G(\tau_0 v_0)}{l_0^2} \cdot \frac{t_0}{q_0}\right]$[a]	Case	N	ρ_0/ρ_m	$\gamma = \left[\frac{2G(\tau_0 v_0)}{l_0^2} \cdot \frac{t_0}{q_0}\right]$
1	1	1/3	0.03125	13	2	1/3	0.03125
2	1	1/3	0.0625	14	2	1/3	0.0625
3	1	1/3	0.125	15	2	1/3	0.125
4	1	1/3	0.25	16	2	1/3	0.25
5	1	1/5	0.03125	17	2	1/5	0.03125
6	1	1/5	0.0625	18	2	1/5	0.0625
7	1	1/5	0.125	19	2	1/5	0.125
8	1	1/5	0.25	20	2	1/5	0.25
9	1	1/8	0.03125	21	2	1/8	0.03125
10	1	1/8	0.0625	22	2	1/8	0.0625
11	1	1/8	0.125	23	2	1/8	0.125
12	1	1/8	0.25	24	2	1/8	0.25

[a] The flow rate, speed and time scales are $q_0 = \rho_* v_f$, $v_0 = l_0/t_0$, $t_0 = l_0 \rho_m / q_0$, respectively.

work of Smirnova, et al. (2017), Zhang's model can be written as

$$\begin{cases} \rho_t + q_x = 0, \\ q_t + \{q^2/\rho + p + [(2\beta c_0) \cdot (c/c_0)](q/\rho)\}_x = R, \\ R = [\frac{(q_e - q)}{\tau_0}](c/c_0) + [(2\beta c_0) \cdot (c/c_0)\rho](q/\rho)_{xx} + (q/\rho)[(2\beta c_0) \cdot (c/c_0)\rho]_x. \end{cases} \tag{32}$$

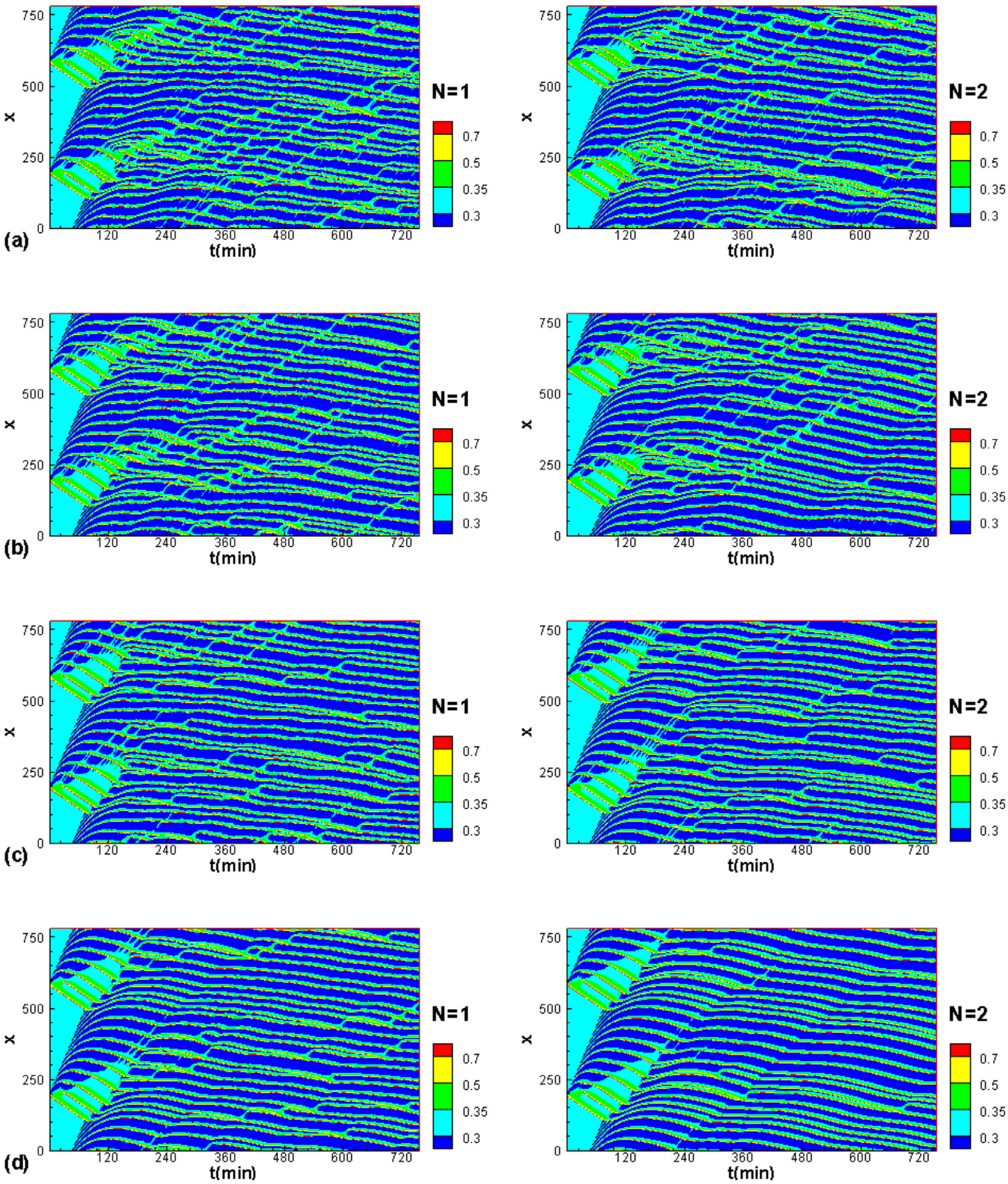

Fig. 7. Spatial-temporal evolutions of ring road traffic flow density for ρ_0/ρ_m=1/3, (a) γ=0.03125, (b) γ=0.0625, (c) γ=0.125, and (d) γ=0.25.

where equilibrium flow rate q_e satisfies Eq. (8), sound speed ratio c/c_0 is described by Eq. (19), with traffic pressure calculated by Eq. (20). The dimensionless parameter β is given by

$$\beta = \frac{\nu}{2\tau_0 c_0^2}. \tag{33}$$

The numerical method for Eq. (32) is also TVD (Roe, 1981) as described in Section 3. It is noted that the discretization of $[(2\beta c_0)\cdot(c/c_0)\rho]_x$ is implemented by a second order upwind scheme (Tao, 2001).

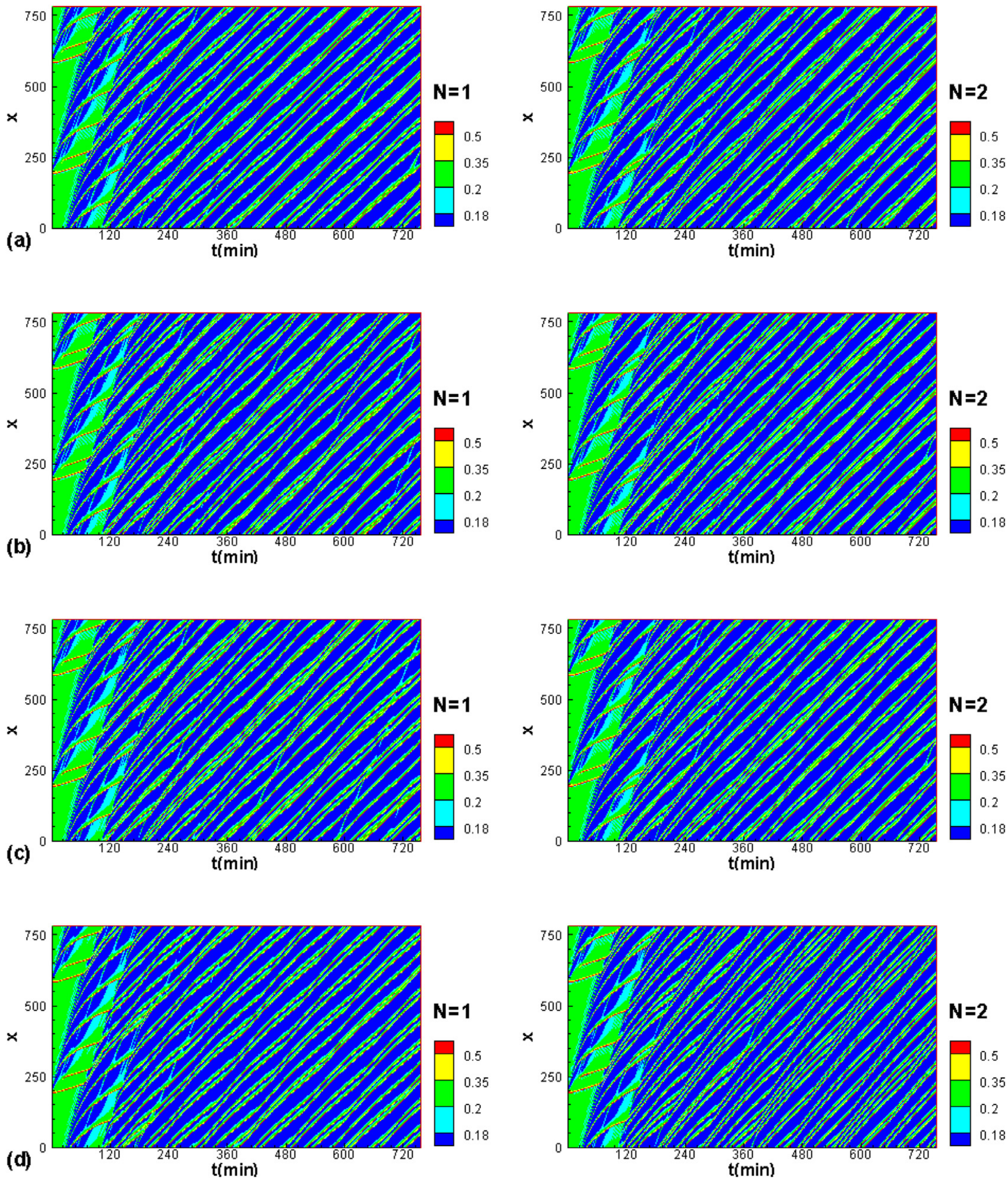

Fig. 8. Spatial-temporal evolutions of ring road traffic flow density for ρ_0/ρ_m=1/5, (a) γ=0.03125, (b) γ=0.0625, (c) γ=0.125, and (d) γ=0.25.

4.1. Parameters and conditions

Using the viscoelastic models and Zhang's model (Zhang, 2003), numerical simulations of ring traffic flows are performed for validation. The road length is x_{lmax}=780, with a length unit l_0 =160 m, a velocity scale $v_0 = v_f\rho_*/\rho_m \approx 3.176$ m/s, and time scale $t_0 = l_0/v_0 (\approx 50.377$ s). Other parameters, including free flow speed, jam density, braking distance and average length of vehicles are given in Table 1, and the 1st critical density ρ_* is obtained from Eq. (10). The second critical speed is assumed to be 15 km/h (Zhu and Yang, 2013), which gives $\Lambda = 3.239,\ \rho_{c2} = 0.7344$. When the average vehicle length l and jam density ρ_m given in Table 1 are used, the dimensionless parameter α has a value 0.87, for which the dependence of traffic pressure p and sound speed ratio c/c_0 on density ρ/ρ_m are shown in Fig. 2.

The blue-colored curve (a) indicates that traffic pressure increases with density monotonically, for $\alpha = 0.87$, from $p = 0$ when there is no vehicles on the road to $p_m = 0.1957$ where the road is completely jammed $\rho = 1$. For all free flow states

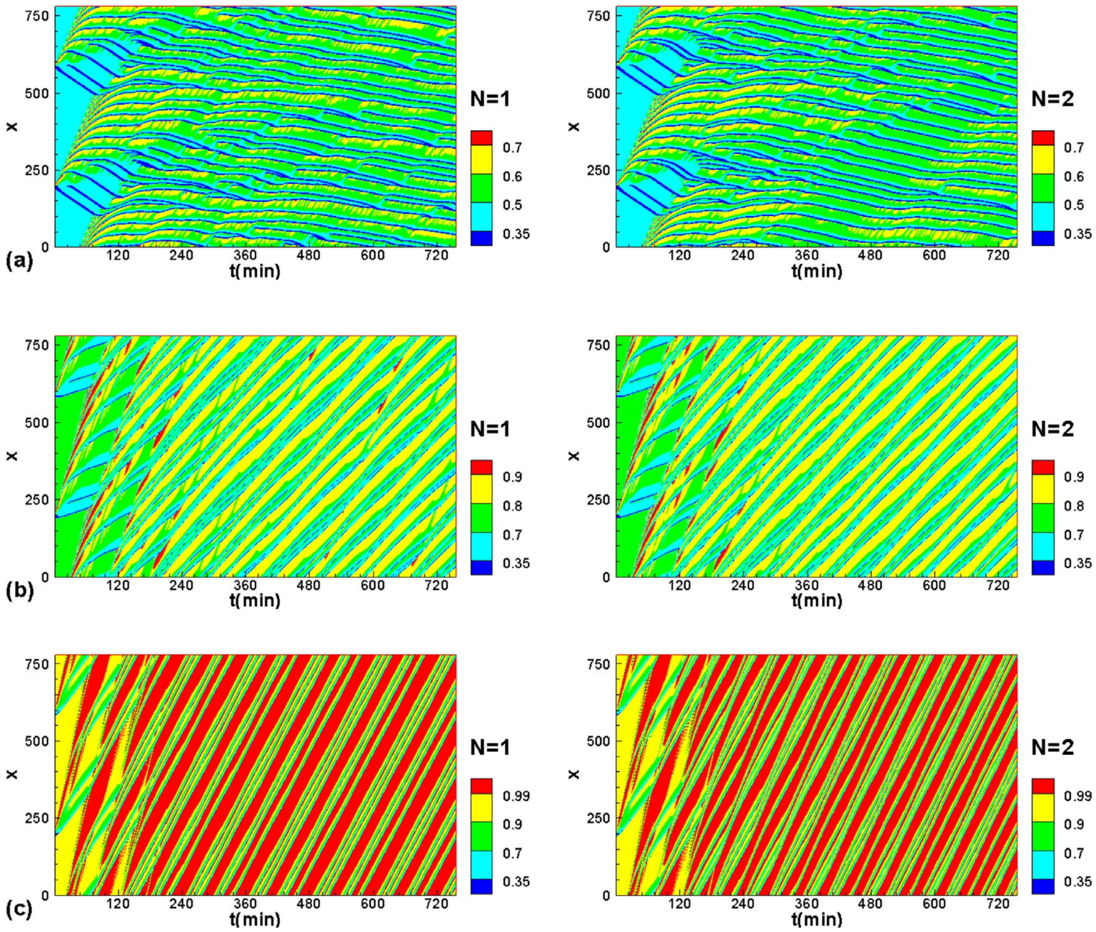

Fig. 9. Spatial-temporal evolutions of ring road traffic flow speed for γ=0.0625, (a) ρ_0/ρ_m=1/3, (b) ρ_0/ρ_m=1/5, (c) ρ_0/ρ_m=1/8.

$\rho \le \rho_*$, $\rho_* = 0.1039$, traffic pressure p holds a value less then 0.2905%; for unsaturated traffic flows $\rho \in (\rho_*, \rho_s)$, with the saturation point $\rho_s = 1/e \approx 0.368$, e=2.71828, p holds a value in the range (0.2905%, 1.375%); for over-saturated traffic flows having a density less than the second critical density $\rho_{c2} = 0.666$, $\rho \in [\rho_s, \rho_{c2})$, p has a value located in the range [1.375%, 5.174%). It can be seen that the second critical pressure $p_{c2} = 5.174\%$, beyond which the pressure increases rapidly with traffic density, it reaches a value of about 0.1957 for $\rho = 1$.

The black curve (b) indicates that traffic sound speed c measured by the second critical sound speed c_0 also increase with traffic density monotonically. Even for the case when the road is empty, sound speed has a value of 0.3611. On the other hand, when traffic flow is completely jammed, it is approximately equal to 2.777. In particular, at traffic saturation point ρ_s, $c/c_0 = 0.531$.

It is noted that the value of artificial parameter ϵ_k is set at 0.05, which is used to evaluate the coefficients of viscous term $Q_k(z)$ in the prediction of numerical flux $\hat{\mathbf{F}}_{i+1/2}$. The term $Q_k(z)$ is defined by

$$Q_k(z) = \begin{cases} |z|, & \text{For } |z| > \epsilon_k; \\ \frac{1}{2}(z^2 + \epsilon_k^2)/\epsilon_k, & \text{Otherwise.} \end{cases}$$

An increase in numerical viscosity can lead to the shock profile of the reproduced wide moving jam in conserved higher-order traffic flow model (Zhang, et al., 2009) becomes smoother and the backward moving wave becomes faster (Qiao et al. (2014). However, numerical viscosity effects in traffic flow simulations are not obvious, as shown by the numerical work of Delis, et al. (2014), the deviation of the calculated traffic flow curves based on a second-order MUSCL (i.e., monotone upstream-centered scheme for conservation laws) scheme and a fifth-order WENO scheme is rather small, visually difficult to distinguish. Since the source term used to describe traffic acceleration has been handled with linear expansion to improve temporal discretization accuracy, the numerical viscosity effects in the present numerical tests should be as small as negligible.

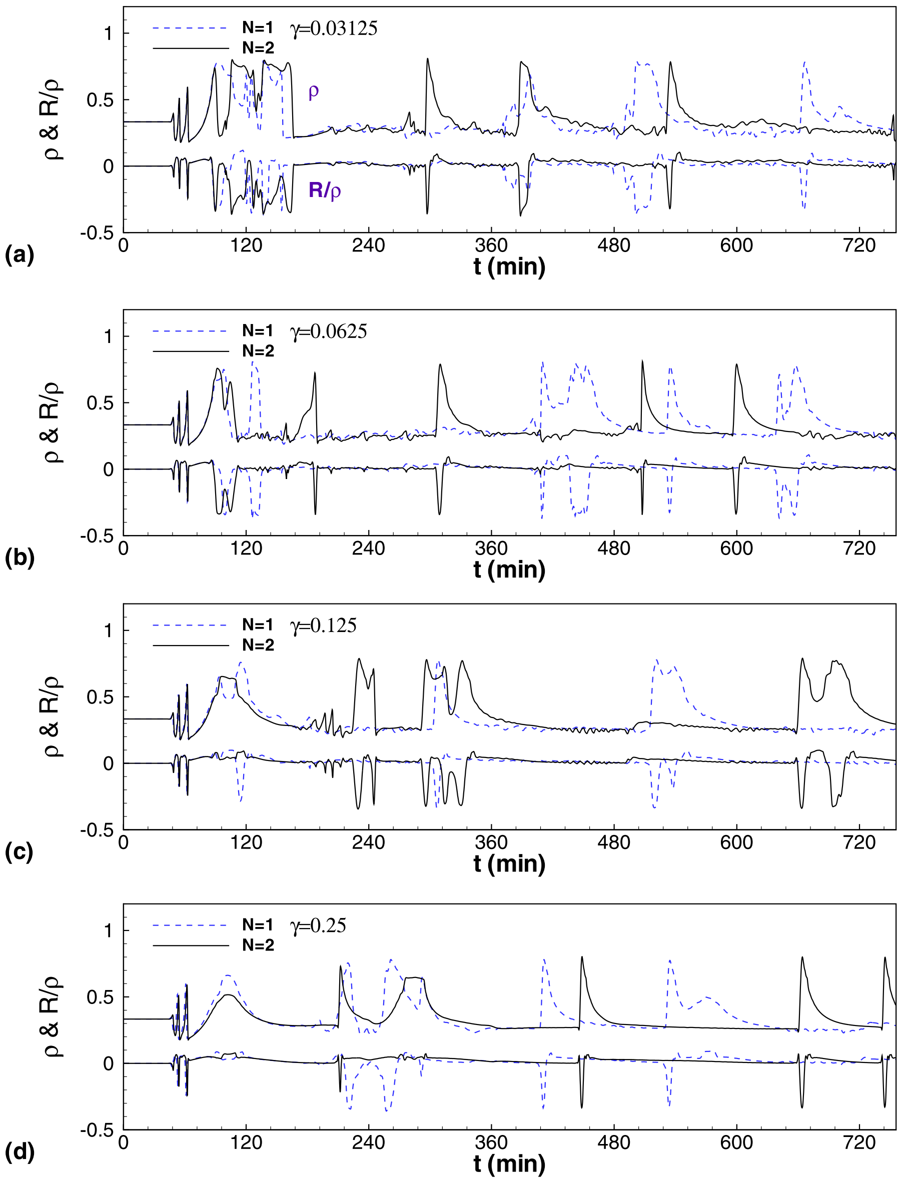

Fig. 10. Temporal evolutions of traffic flow density and acceleration at x=390 for ρ_0/ρ_m=1/3; (a) γ=0.03125, (b) γ=0.0625, (c) γ=0.125, and (d) γ=0.25. Note that R/ρ has a unit of the permitted maximum acceleration 1.5 m/s^2 as reported by Smirnova, et al. (2015).

Initial density condition is assumed to be

$$\rho(0,x)=\begin{cases}1.0, & \text{for} x\in[x_I-1,x_I+1],\\ \rho_0/\rho_m, & \text{Otherwise,}\end{cases} \tag{34}$$

with $q(0,x)=q_e(\rho(0,x))$. As shown in Fig. 3, x_I $(I=A,B)$ is calculated from values given in Table 1, with Reynolds number ($\mathrm{Re}=l_0 v_0/\nu$) of 8, and $2\beta=2.941\times10^{-2}$. The viscoelasticity parameter denoted by $\gamma=\left[\frac{2G(\tau_0 v_0)}{l_0^2}\cdot\frac{t_0}{q_0}\right]$, has a value of 0.125 (Smirnova, et al., 2017). The model validation is based on the comparison of numerical simulations of ring traffic flows for two cases of ρ_0/ρ_m=1/3 and 1/5.

4.2. Comparison of results

Traffic flow patterns in the $t-x$ plane given by density contours are shown in Fig. 4, where (a) shows the flow patterns based on Zhang's model (2003), while (b) and (c) show the patterns based on viscoelastic models for N=1, 2 respectively. The density in the blue region is less than 0.3, while in the red region it is higher than 0.7, with the cyan region having

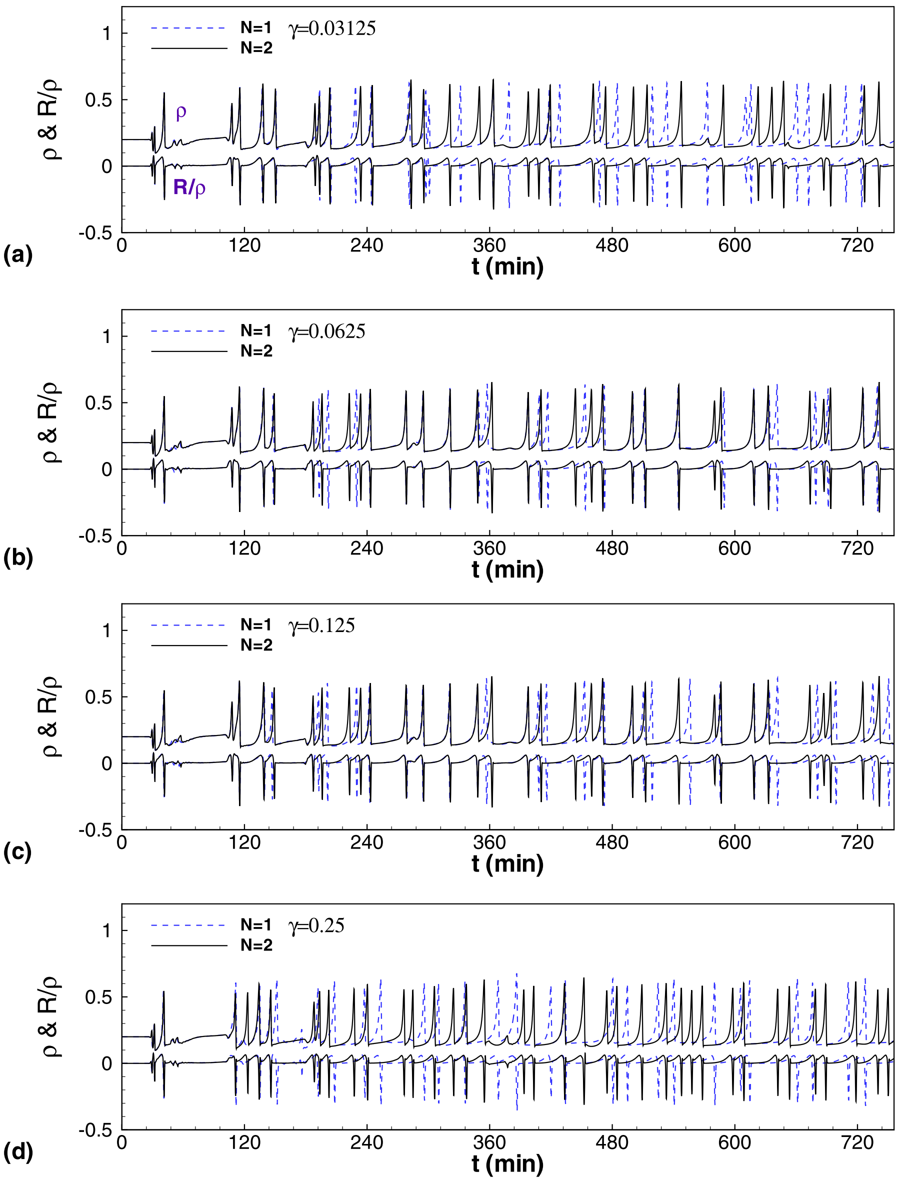

Fig. 11. Evolutions of traffic flow density and acceleration at x=390 for ρ_0/ρ_m=1/5; (a) γ=0.03125, (b) γ=0.0625, (c) γ=0.125, and (d) γ=0.25. Note that R/ρ has a unit of the permitted maximum acceleration 1.5 m/s^2 as reported by Smirnova, et al. (2015). (For interpretation of the references to color in this figure, the reader is referred to the web version of this article.)

values in the range of [0.3, 0.35], and the green and yellow regions being in the ranges of [0.35,0.5] and [0.5,0.7] respectively. The similarity to the pattern obtained by Zhang (2003) model, to some extent indicates that viscoelastic traffic flow models are reasonable.

Temporal evolutions of traffic flow speed, density and acceleration for ρ_0/ρ_m=1/3 and 1/5 are shown in Fig. 5 and Fig. 6, respectively. Correspondingly, any negative drop of acceleration (R/ρ) indicates an occurrence of a negative drop of speed (u) , and a positive peak of density (ρ). It can be seen that at the point $x = 390$, the evolutional waves of u, ρ and R/ρ have different shapes, although the pressure and sound speed are kept constant. However, discrepancies between the evolution curves do not justify model reliability, as the absolute value of traffic flow acceleration in the time period $t \in (0,\ 377.8)$ is generally less than unity, which is relevant to its permitted maximum acceleration of 1.5m/s^2.

The model comparison indicates that numerical results based on viscoelastic models are reliable, with the spatial-temporal evolutions reflecting the structures of traffic waves. The numerical results suggest that even for specially light or completely jammed scenarios, the sound speed of traffic flow could be derived.

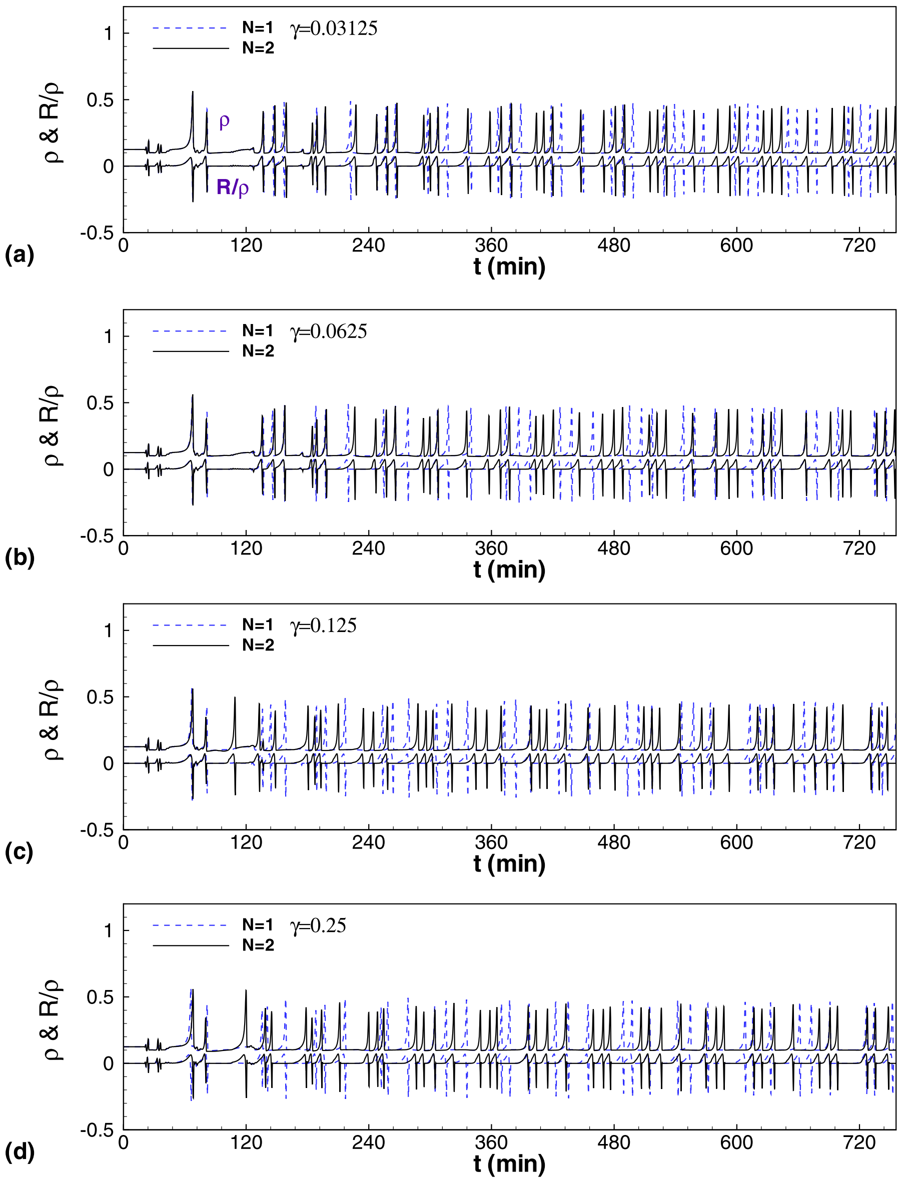

Fig. 12. Evolutions of traffic flow density and acceleration at x=390 for ρ_0/ρ_m=1/8; (a) γ=0.03125, (b) γ=0.0625, (c) γ=0.125, and (d) γ=0.25. Note that R/ρ has a unit of the permitted maximum acceleration 1.5 m/s^2 as reported by Smirnova, et al. (2015).

5. Results and discussion

5.1. Simulation parameters

Using the models described in Section 2, numerical tests are carried out to show the effects of maximum relaxation in predicting ring traffic flows, for which parameters and conditions have been described in Section 4.1. Initial density ρ_0/ρ_m is assigned to be 1/3, 1/5, or 1/8 in the numerical tests, as shown in Table 2.

The initial density ρ_0/ρ_m can be slightly lower than saturation density $\rho_s(=\rho_m/e)$; has value of between the 1st critical density ρ_* and the saturation density ρ_s; or be slightly higher than ρ_*. Hence, under the initial conditions for the 24 cases in Table 2, the spatial-temporal evolutions of the irregularity of initial density can lead to the generation of traffic shock waves, with the propagation and interaction with rarefaction waves forming traffic flow patterns sensitive to the viscoelasticity $\gamma\left(=\left[\frac{2G(\tau_0 v_0)}{l_0^2}\cdot\frac{t_0}{q_0}\right]\right)$, as reported recently (Smirnova, et al., 2017).

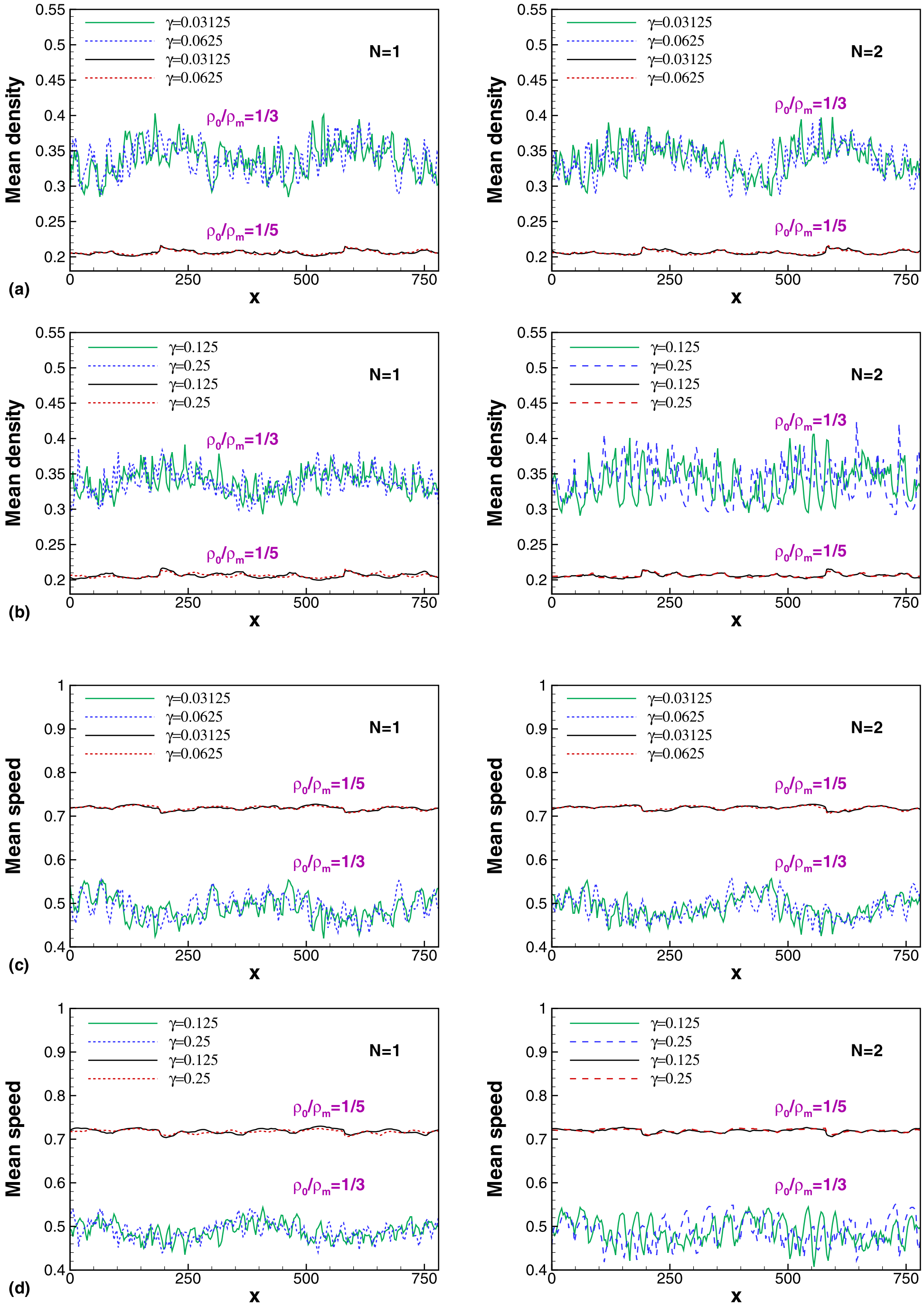

Fig. 13. Distributions of mean density (a–b) and speed (c–d) on the single lane ring road for ρ_0/ρ_m=1/3, 1/5.

5.2. Traffic flow patterns

For ρ_0/ρ_m=1/3, traffic flow patterns illustrated by density contours in the $t-x$ plane are shown in Fig. 7 for maximum relaxation N=1 (left) and $N=2$ (right). The density contours shown in (a–d) in the Flood-type form are labeled by values of 0.3, 0.35, 0.5, and 0.7 respectively. Similar to what experimentally observed in German highways (Kerner, 1998), the patterns given by Fig. 7 reveal that there are spontaneously generated jams, which occurred between the two initial jams started spreading from the points near X_A and X_B. The spontaneous jams start to propagate forward, but for the leading one

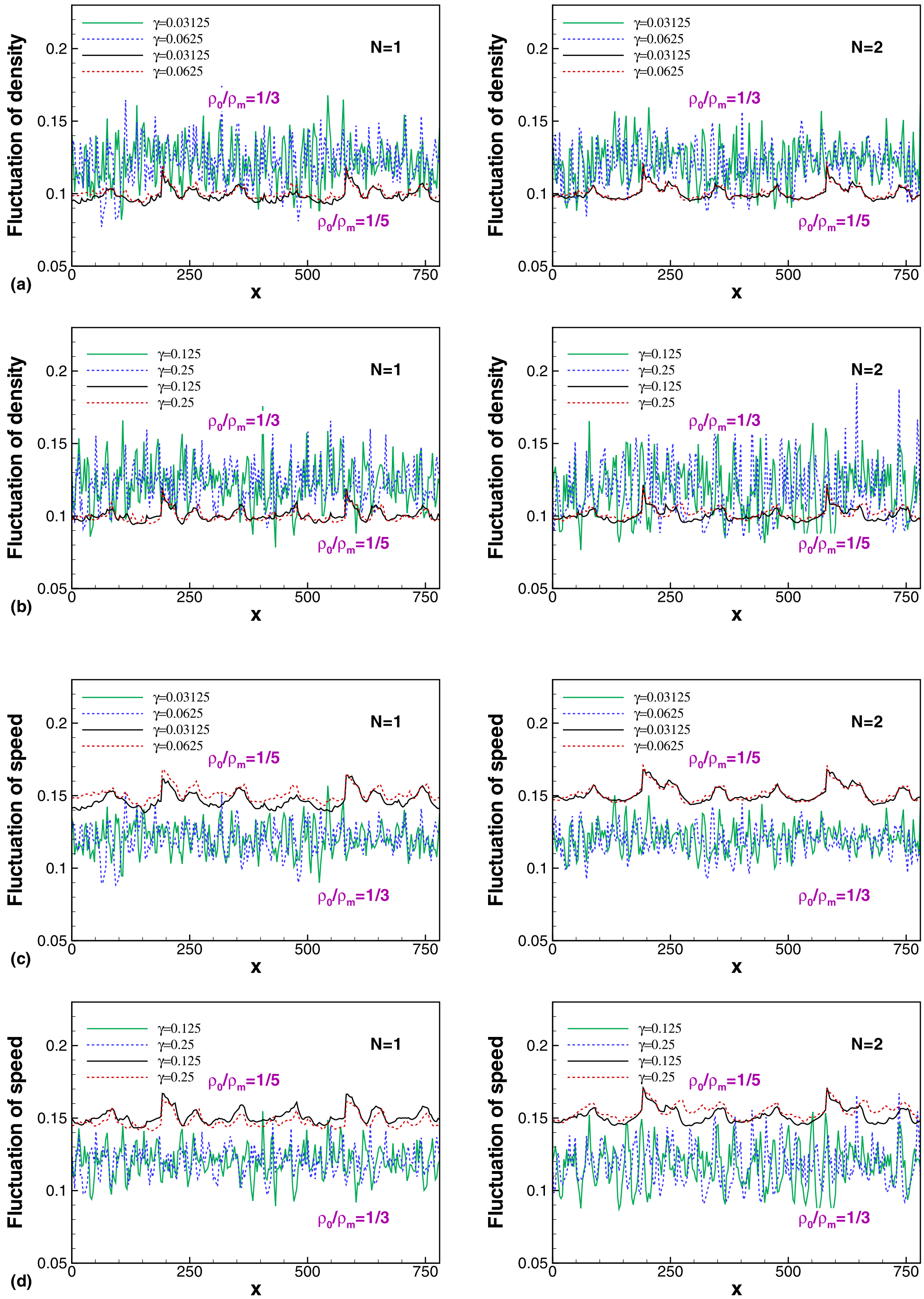

Fig. 14. Distributions of fluctuations of density (a–b) and speed (c–d) on the single lane ring road for ρ_0/ρ_m=1/3, 1/5.

nearest to initially originated jam, its mergence with the backward spreading initial jam, makes a change of propagating direction for the merged jam. The spontaneous jams promote traffic flow to enter into a self-organized stop-and-go mode.

In initial period $t \in (0, 150)$, the traffic shock waves propagate forward and backward. However, with the evolutions and interactions of traffic waves, when the evolution time is greater than 150 minutes, almost all traffic shocks on the ring road propagate backward, as can be observed by tracing the temporal evolution of higher density contours in Fig. 7(a–d).

With the increase of viscoelastic parameter γ, self-organizing ability of the ring- traffic flows increases, the traffic flow pattern becomes more regular as a result of interaction of traffic shock and rarefaction waves. This indicates that self-organizing ability plays a crucial role in traffic flow pattern formation. Furthermore, the traffic flow pattern is rather sensitive

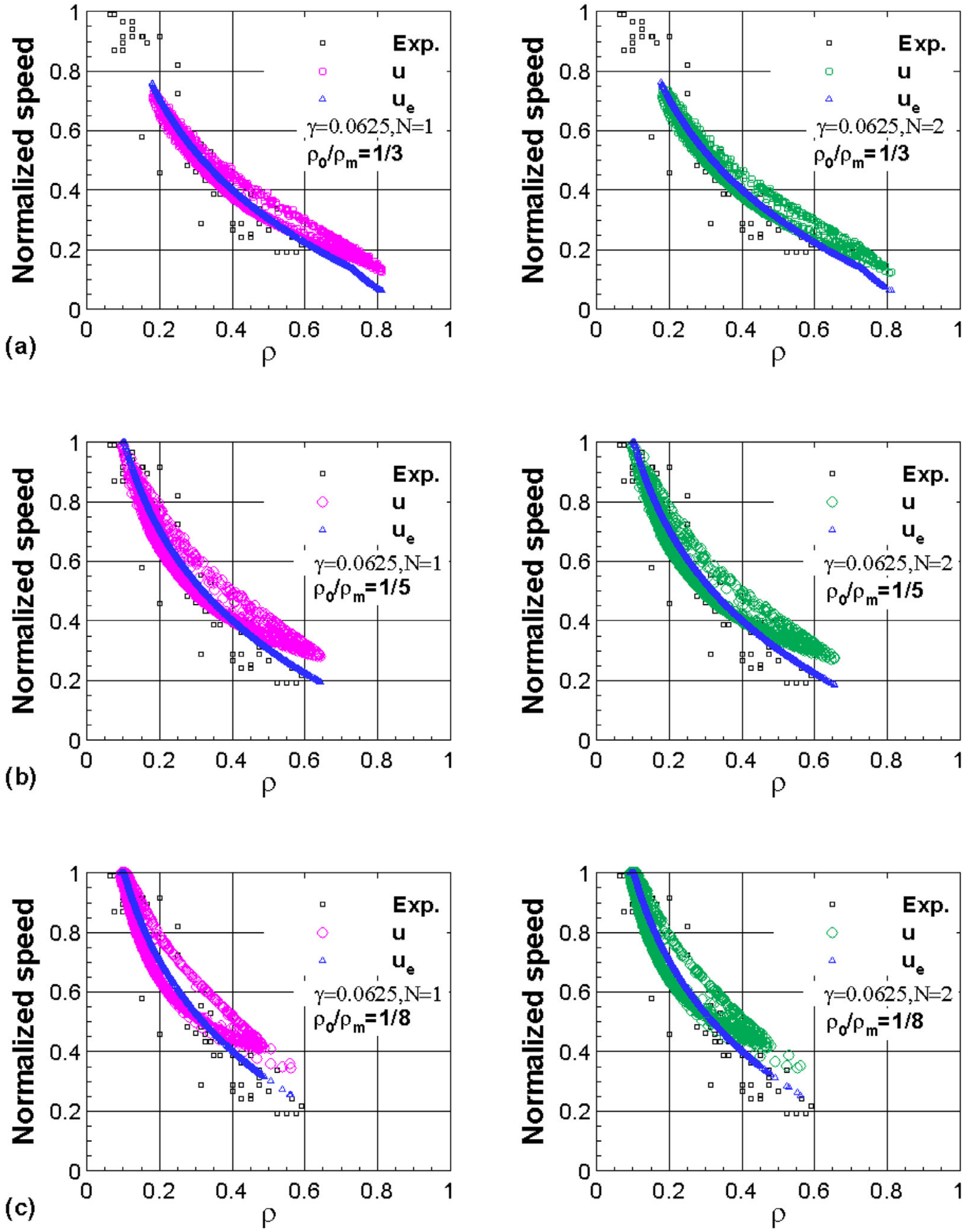

Fig. 15. Comparison of traffic speed with existing measured data at $x = 390$ for γ=0.0625; (a) ρ_0/ρ_m=1/3, (b) ρ_0/ρ_m=1/5, (c) ρ_0/ρ_m=1/8. The observation data are obtained from McShane et al. (1998), and the jam density for normalisation is supposed to be 200 veh/mile.

to the maximum relaxation (N) of traffic flow modeling, indicating that the numerically simulated traffic shock intensity, shock propagation speed and spreading direction, as well as the rarefaction wave properties all depend on the maximum relaxation (N).

On the other hand, as shown in Fig. 8(a–d), traffic flow patterns on the ring road are extremely dependent on initial density ρ_0/ρ_m, which examines the spatial averaged density on the ring-road. It is seen that for ρ_0/ρ_m=1/5, independent of the value of γ, all shock waves propagate forward, with the propagation speeds closely relating to the wave interaction and the fundamental diagram used in the numerical test, as explained by Daganzo (1997) and recent works (Lebacque, et al., 2007; Zhang, Wong and Dai, 2009; Lebacque and Khoshyaran 2013; Smirnova, et al., 2017). Furthermore, different relaxation choice of N leads to different flow patterns illustrated by density contours.

The extreme dependence of traffic flow patterns on initial density ρ_0/ρ_m can also be seen from the patterns depicted by spatial-temporal evolutions of speed shown in Fig. 9(a–c). The shock wave spreading direction are observed by tracing the evolution of lower speed contours. As seen in Fig. 9(c), for ρ_0/ρ_m=1/8, the spatial averaged density on the ring road is close to the 1st critical density ρ_*/ρ_m, all the shock waves propagate forward, but having faster propagation speeds than that for ρ_0/ρ_m=1/5, due to higher gradients of the speed contours. Similarly, the difference caused by the choice of relaxation maximum N can be observed again from flow patterns given in Fig. 9(c).

5.3. Evolutions of speed and acceleration

To observe the difference caused by the choice of N more directly, temporal evolutions of density (ρ) and acceleration (R/ρ) at x=390 are illustrated in Figs. 10(a–d), 11(a–d), and 12(a–d), where the density is measured by the jam density ρ_m, and the acceleration unit is permitted maximum acceleration of 1.5m/s^2 as reported by Smirnova, et al. (2015). The evolutions of ρ and R/ρ have a synchronized property, any negative drop of acceleration (R/ρ) accompanies with a sharp peak of traffic density (ρ), as shown in Figs. 10–12. Such evolution behavior between acceleration and density is influenced by viscoelasticity γ, initial density ρ_0/ρ_m, and relaxation maximum N.

As shown in Fig. 10(a–d), corresponding to the density contours given in Fig. 7(a–d), any negative acceleration drop implies an occurrence of traffic shock wave. In contrast, any smooth part of evolution curve of R/ρ indicates that there is a comparatively steady moving trend of vehicles motion at the observing point $x = 390$. Characterized by the traffic shock wave structures on the ring-road, the density ρ at $x = 390$ oscillates around a mean value close to 1/3. In most cases, acceleration R/ρ keeps a value close to zero except for the negative jumps with a height of about 0.35, suggesting that the simulation parameters in the numerical tests are appropriate. This implies that when acceleration is beyond the limit as reported by Smirnova, et al. (2015), the simulation results become unreliable.

The temporal evolutions of density ρ and acceleration R/ρ denoted by blue-dashed curves for N=1, do not overlap with the evolutional solid curves for N=2, and such effects of maximum relaxation on temporal evolutions of ρ and R/ρ at x=390 can be seen more clearly than that for the differences between traffic patterns given in Fig. 7(a–d).

Coinciding with traffic patterns given in Figs. 8(a–d), 11(a–d) show the temporal evolutions of density and acceleration at x=390 for ρ_0/ρ_m=1/5. In comparison with Figs. 10, it can be seen that the temporal evolutional behaviors of ρ and R/ρ are under the influence of initial density, the ρ_0/ρ_m decrease of 1/3 $\rightarrow$ 1/5, not only brings about a decrease of density peak value and a slight drop approximately from 0.35 to 0.3 of negative drop height of R/ρ, but also an increase of occurrent frequency of negative drop of R/ρ. Again, the apparent separations of dashed-blue curves from solid curves in Fig. 11(a–d) indicate the differences caused by N.

Similarly, when ρ_0/ρ_m=1/8, from Fig. 12(a–d) it is seen that the temporal evolutions of density coincide with the flow pattern given by speed contours in Fig. 9(c). Again, the differences caused by N can be seen clearly. In addition, when initial density ρ_0/ρ_m changes from 1/5 to 1/8, the negative drop of the R/ρ curve decreases approximately from 0.3 to 0.25.

5.4. Distributions of density and speed

By averaging the traffic density and speed over a time period of about 755 minutes, the mean traffic density and mean traffic speed on the ring road can be obtained. For ρ_0/ρ_m=1/3, and 1/5, the relevant distributions are shown in Fig. 13(a–d) for N=1, 2 with γ=0.03125, 0.0625, 0.125, and 0.25. The distributions of mean traffic density and speed on the single lane ring road are both sensitive to viscoelasticity γ, leading to explicitly different distributions of mean traffic density and speed. This confirms to the finding that there exists a wide spectrum of pattern formation phenomena in traffic systems, as previously reported by other traffic flow models, such as car-following models, cellular automaton models (Nagel, et al., 1992; Helbing and Huberman, 1998; Chowdhury, et al., 2000), gas-kinetic models and fluid-dynamical models (Nagatani, 2002).

In Fig. 13(a–b), it is seen that on the ring-road, the mean density oscillates around a value just slightly over the initial density ρ_0/ρ_m, with two initial traffic jams around x_A and x_B. The magnitude of spatial oscillation is very sensitive to the initial density value and the decrease of initial density leads to an acute drop of the spatial variation magnitude as shown in Fig. 13(c–d).

To show the characteristics of the ring road traffic flow in more details, the distributions of density and speed fluctuations are shown in Fig. 14(a–d), here the fluctuation refers to time-average based root mean square (RMS) value of some variable. It can be seen that density and speed fluctuations are consistent with the patterns in Figs. 7(a–d), and 8(a–d). The fluctuations of ρ and u are not only sensitive to viscoelasticity γ and initial density ρ_0/ρ_m, but also closely dependent on the maximum relaxation N. As fluctuations reflect the interaction of shocks and traffic rarefaction waves, the change of γ, ρ_0/ρ_m, or N causes differences in density and speed fluctuations.

As shown in Fig. 15(a–d), the instantaneous traffic speed (u) at x=390 is illustrated as a function of traffic density. Instantaneous equilibrium speed (u_e) at x=390 determined by Eq. (8) is labeled by unfilled triangles, with measured data of McShane et al. (1998) labeled by unfilled black squares. The comparison of speed-density relation at a given section with measured data, shows the ring road traffic flows are sensitive to initial density ρ_0/ρ_m, indicating that viscoelastic traffic flow modeling gives reliable simulation results.

6. Conclusions

In analogous to non-Newtonian fluid flow, a viscoelastic traffic flow modeling is used to predict the effects of maximum relaxation on ring- road traffic flows numerically. The following findings are obtained:

1. As self-organizing ability of traffic flows increases with the increase of viscoelasticity, the traffic flow pattern becomes more regular, indicating that traffic flow self-organization plays a crucial role in the determination of traffic flow patterns, while the maximum relaxation brings about some effects in the pattern evolution and the interaction between traffic shocks and rarefaction waves.
2. The simulation parameters adopted in the numerical tests for ring road traffic flows are appropriate. For unsaturated ring traffic flows with two initial jams, there are spontaneous generated jams appearing between initial jams. The spontaneous jams promote the occurrence of stop-and-go traffic mode.
3. The distributions of the mean and RMS values of traffic density and speed on the ring road indicate that the characteristics of traffic flows on the ring road depends on the initial density. For denser ring road traffic flows, almost all traffic shocks propagate backward. When the initial density becomes smaller, traffic shocks propagate forward. When the initial density is close to but higher than the 1st critical density, the ring road traffic flow keeps in free flow state.
4. The maximum relaxation in viscoelastic traffic flow modeling does lead to some differences in patterns depicted by spatial-temporal evolution of density or speed. In addition, numerical tests reveals that the maximum relaxation causes a small variation of traffic flow patterns.

Acknowledgments

This work is supported by NSFC (10972212).

References

Aw, A., Rascle, M., 2000. Resurrection of *second order* models of traffic flow. SIAM J. Appl. Math. 60, 916–938.
Bogdanova, A., Smirnova, M.N., Zhu, Z.J., Smirnov, N.N., 2015. Exploring peculiarities of traffic flows with a viscoelastic model. Transportmetr. A Transp. Sci. 11 (7), 561–578.
Chang, G.L., Zhu, Z.J., 2006. A macroscopic traffic model for highway work zones: formulations and numerical results. J. Adv. Transp. 40 (3), 265–287.
Chowdhury, D., Santen, L., Schadschneider, A., 2000. Statistical physics of vehicular traffic and some related systems. Phys. Rep. 329, 199–329.
Costeseque, G., Lebacque, J.P., 2014. A variational formulation for higher order macroscopic traffic flow models: numerical investigation. Transp. Res. Part B Methodol. 70, 112–133.
Daganzo, C.F., 1995. Requiem for second-order fluid approximations of traffic flow. Transp. Res. Part B Methodol. 29, 277–286.
Daganzo, C.F., 1997. Traffic flow theory. In: Daganzo, C.F. (Ed.), Fundamentals of Transportation and Traffic Operations. Pergamon, New York, pp. 67–160.
Daganzo, C.F., 2002a. A behavioral theory of multi-lane traffic flow. part i: long homogeneous freeway sections. Transp. Res. Part B Methodol. 36, 131–158.
Daganzo, C.F., 2002b. A behavioral theory of multi-lane traffic flow: part ii: merges and onset of congestion. Transp. Res. Part B Methodol. 36, 159–169.
Delis, A.I., Nikolos, I.K., Papageorgiou, M., 2014. High-resolution numerical relaxation approximations to second-order macroscopic traffic flow models. Transp. Res. Part C Emerg. Technol. 44, 318–349.
Greenberg, J.M., 2004. Congestion redux. SIAM J. Appl. Math. 64 (4), 1175–1185.
Haight, F.A., 1963. Mathematical Theories of Traffic Flow. Academic Press, New York.
Han, S.F., 2000. Constitutive theory of viscoelastic fluids. In: Han, S.F. (Ed.), Constitutive Equation and Computational Analytical Theory of Non-Newtonian Fluid. Science Press, Peking, pp. 59–86.
Helbing, D., 1996. Traffic modeling by means of physical concepts. In: D. E. Wolf, M.S., Bachem, A. (Eds.), Proceedings of the Workshop on Traffoc and Granular Flow. World Scientific, Singapore, pp. 87–104.
Helbing, D., 2001. Traffic and related self-driven many-particle systems. Rev. Mod. Phys. 73 (4), 1067–1414.
Helbing, D., Huberman, B.A., 1998. Coherent moving states in highway traffic. Nature 396 (6713), 738–740.
Helbing, D., Treiber, M., 1998. Gas-kinetic-based traffic model explaining observed hysteretic phase transition. Phys. Rev. Lett. 81, 3042–3045.
Hoogendoorn, S.P., Bovy, P.H.L., 2000. Continuum modeling of multiclass traffic flow. Transp. Res. Part B Methodol. 34 (2), 123–146.
Hoogendoorn, S.P., van Wageningen-Kessels, F., Daamen, W., Duives, D.C., Sarvi, M., 2015. Continuum theory for pedestrian traffic flow: local route choice modelling and its implications. Transp. Res. Part C Emerg. Technol. 59, 183–197.
Jin, W.L., Zhang, H.M., 2003. The formation and structure of vehicle clusters in the Payne–Whitham traffic flow model. Transp. Res. Part B Methodol. 37 (3), 207–223.
Kerner, B., Konhäuser, P., 1993. Cluster effect in initially homogemeous traffic flow. Phys. Rev. E 48, 2335–2338.
Kerner, B.S., 1998. Experimental features of self-organization in traffic flow. Phys. Rev. Lett. 81 (17), 3797–3800.
Kerner, B.S., Konhaüser, P., Schilke, M., 1996. A new approach to problems of traffic flow theory. In: Laboratory, T.R. (Ed.), Proceedings of the 13th International Symposium on Transportation and Traffic Theory. July, LYON, FRANCE, pp. 24–26.
Kiselev, A.B., Nikitin, V.F., Smirnov, N.N., Yumashev, M., 2000a. Irregular traffic flow on a ring road. J. Appl. Math. Mech. 64 (4), 627–634.
Kiselev, A.B., Nikitin, V.F., Smirnov, N.N., Yumashev, M.V., 2000b. Irregular traffic flow on a ring road. J. Appl. Math. Mech. 64 (4), 627–634.
Klar, A., Wegener, R., 2000. Kinetic derivation of macroscopic anticipation models for vehicular traffic. SIAM J. Appl. Math. 60 (5), 1749–1766.
Kühne, R. D., 1987. Freeway speed distribution and acceleration noise. In: Gartner, N.H., W. N., Transportation and Traffic Theory. Elsevier: Amsterdam, pp. 119–137.
Kühne, R.D., 1989. Freeway control and incident detection using a stochastic continuum theory of traffic flow. In: Proceedings of the 1st International Conference on Applied Advanced Technology in Transportation Engineering. San Diego, CA, pp. 287–292.
Kühne, R. D., Michalopoulos, P., 2001. Continuum flow models. URL http://www-cta.ornl.gov/cta/research/trb/tft.html
Lebacque, J.P., Khoshyaran, M.M., 2013. A variational formulation for higher order macroscopic traffic flow models of the GSOM family. Transp. Res. Part B Methodol. 57, 245–265.
Lebacque, J.P., Mammar, S., Haj-Salem, H., 2007. Generic second order traffic flow modelling. In: Allsop, R., Benjiamin, G. (Eds.), Transportation and Traffic Theory. Elsevier: Oxford, pp. 755–776.
Li, J., Zhang, H.M., 2013. The variational formulation of a non-equilibrium traffic flow model: theory and implications. Proc. Soc. Behav. Sci. 80, 327–340.
Lighthill, M.J., Whitham, G.B., 1955. On kinematic waves ii: a theory of traffic flow on long crowded roads. Proc. Roy. Soc. Lond. A 229, 317–345.
LiuG. Q., Lyrintzis, A. S., P.G.M., 1996. Modelling of freeway merging and diverging flow dynamics. Appl. Math. Model. 229, 317–345.
Lyrintzis, A.D., Liu, G., Michalopoulos, P.G., 1994. Development and comparative evaluation of high-order traffic flow models. Transp. Res. Rec. 1547, 174–183.

Mammar, S., Lebacque, J.P., Salem, H.H., 2009. Riemann problem resolution and Godunov scheme for the Aw-Rascle-Zhang model. Transp. Sci. 43 (4), 531–545.
McShane, W.R., Roess, R.P., Prassas, E.S., 1998. Calibration relationships for freeway analysis. In: McShane, W.R., Roess, R.P., Prassas, E.S. (Eds.), Traffic Engineering. Prentice-Hall: New Jersey, pp. 282–306.
Nagatani, T., 2002. The physics of traffic jams. Rep. Prog. Phys. 65, 1331–1386.
Nagel, K., Schreckenberg, M., 1992. A cellular automaton model for freeway traffic. J. Phys. I 2 (12), 2221–2229.
Ngoduy, D., 2012. Application of gas-kinetic theory to modelling mixed traffic of manual and adaptive cruise control vehicles. Transportmetr. Part A Transp. Sci. 8 (1), 43–60.
Ngoduy, D., 2013. Platoon-based macroscopic model for intelligent traffic flow. Transportmetr. B Transp. Dyn. 1 (2), 153–169.
Ou, Z.H., Dai, S.Q., Zhang, P., Dong, L., 2007. Nonlinear analysis in the Aw-Rascle anticipation model of traffic flow. SIAM J. Appl. Math. 67 (3), 605–618.
Paveri-Fontana, S.L., 1975. On Boltzmann-like treatments for traffic flow: a critical review of the basic model and an alternative proposal for dilute traffic analysis. Transp. Res. Part B Methodol. 9, 225–235.
Payne, H., 1979. Freflo: a macroscopic simulation model for freeway traffic. Transp. Res. Rec. 772, 68–75.
Payne, H.J., 1971. Models of freeway traffic and control. Math. Model Publ. Syst. Simul. Council Proc. La Jola Calif. 1, 51–61.
Qiao, D.L., Zhang, P., Wong, S.C., Choi, K., 2014. A variational formulation for higher order macroscopic traffic flow models of the GSOM family. Appl. Math. Comput. 244, 567–576.
Rascle, M., 2002. An improved macroscopic model of traffic flow: derivation and links with the Lighthill-Whitham model. Math. Comput. Model. 35, 581–590.
Richards, P.I., 1956. Shock waves on the freeway. Oper. Res. 4, 42–51.
Roe, P.C., 1981. Approximate Riemann solver, parameter vectors, and difference schemes. J. Comput. Phys. 43, 357–372.
Shui, H.S., 1998. TVD scheme. In: Shui, H.S. (Ed.), Finite Difference in One-dimensional Fluid Mechanics. National Defense: Beijing, in Chinese, pp. 333–355.
Smirnov, N.N., Kiselev, A.B., Nikitin, V.F., SilnikovM.V., Manenkova, A.S., 2014. Hydrodynamic traffic flow models and its application to studying traffic control effectiveness. WSEAS Trans. Fluid Mech. 9, 178–186.
Smirnova, M.N., Bogdanova, A.I., Smirnov, N.N., Kiselev, A.B., Nikitin, V.F., Manenkova, A.S., 2018. Unsteady-state traffic flow models for urban regulation strategy planning. Archit. Urban Des. in press.
Smirnova, M.N., Bogdanova, A.I., Zhu, Z.J., Smirnov, N., 2016. Traffic flow sensitivity to visco-elasticity. Theor. Appl. Mech. Lett. 6, 182–185.
Smirnova, M.N., Bogdanova, A.I., Zhu, Z.J., Smirnov, N., 2017. Traffic flow sensitivity to parameters in viscoelastic modelling. Transportmetr. B Transp. Dyn. 5 (1), 115–131.
Smirnova, M.N., Bogdanova, A.I., Zhu, Z.J., Manenkova, A.S., Smirnov, N.N., 2014a. Mathematical modeling of traffic flows using continuum approach. visco-elastic effect in traffic flows. Math. Model. 26 (7), 54–64 (InRussian).
Spiliopoulou, A., Kontorinaki, M., Papageorgiou, M., Kopelias, P., 2014. Macroscopic traffic flow model validation at congested freeway off-ramp areas. Transp. Res. Part C Emerg. Technol. 41, 18–29.
Spiliopoulou, A., Papamichail, I., Papageorgiou, M., Tyrinopoulos, I., Chrysoulakis, J., 2015. Macroscopic traffic flow model calibration using different optimization algorithms. Transp. Res. Proc. 6, 144–157.
Tao, W.Q., 2001. Numerical Heat Transfer. Xi'an Jiantong University Press: Xi'an (in Chinese), pp. 25–251.
Tordeux, A., Roussignol, M., Lebacque, J.P., Lassarre, S., 2014. A stochastic jump process applied to traffic flow modelling. Transportmetr. A Transp. Sci. 10 (4), 350–375.
Treiber, M., Hennecke, A., Helbing, D., 1999. Derivation, properties, and simulation of a gas-kinetic-based, nonlocal traffic model. Phy. Rev. E 59 (1), 239–253.
Wagner, M.H., 1978. Constitutive analysis of uniaxial elongational flow data of a low-density polyethylene melt. J. Non-Newton. Fluid Mech. 4 (1–2), 39–55.
Whitham, G.B., 1974. Linear and Nonlinear Waves. Wiley, NewYork.
Wong, G.C.K., Wong, S.C., 2002. A multi-class traffic flow model-an extension of LWR model with heterogeneous drivers. Transp. Res. Part A Policy Pract. 36, 827–841.
Xu, R.Y., Zhang, P., Dai, S.C., Wong, S.C., 2007. Admissibility of a wide cluster solution inanisotropic higher-order traffic flow models. SIAM J. Appl. Math. 68 (2), 562–573.
Zhang, H.M., 1998. A theory of nonequilibrium traffic flow. Transp. Res. Part B Methodol. 32 (7), 485–498.
Zhang, H.M., 2003. Driver memory, traffic viscosity and a viscous vehicular traffic flow model. Transp. Res. Part B Methodol. 37, 27–41.
Zhang, P., Wong, S.C., 2006. Essence of conservation forms in the travelling wave solutions of higher-order traffic flow. Phys. Rev. E 74 (2), 026109.
Zhang, P., Wong, S.C., Dai, S.Q., 2009. A conserved higher order aniso-tropic traffic flow model: description of equilibrium and non-equilibrium flows. Transp. Res. Part B Methodol. 43 (5), 562–574.
ZhangP., Wong, S.C., C.W.S., 2006. A weighted essentially non-oscillatory numerical scheme for a multi-class traffic flow model on an inhomogeneous highway. J. Comput. Phys. 212 (2), 739–756.
Zhu, Z.J., Wu, T.Q., 2003. Two-phase fluids model for freeway traffic and its application to simulate the evolution of solitons in traffic. ASCE J. Transp. Eng. 129, 51–56.
Zhu, Z.J., Yang, C., 2013. Visco-elastic traffic flow model. J. Adv. Transp. 47, 635–649.